Correlations to improve high-temperature strength and room temperature ductility of refractory complex concentrated alloys

Oleg N. Senkov, Stéphane Gorsse, Daniel B. Miracle, Rao I. S., Todd M. Butler

Materials & Design 239 (2024) 112762

Contents lists available at ScienceDirect

Materials & Design

journal homepage: www.elsevier.com/locate/matdes

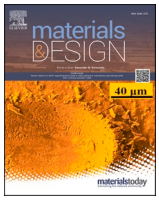

Correlations to improve high-temperature strength and room temperature ductility of refractory complex concentrated alloys

O.N. Senkov [a,b,*], S. Gorsse [c], D.B. Miracle [a], S.I. Rao [a,b], T.M. Butler [a]

[a] Air Force Research Laboratory, Materials and Manufacturing Directorate, Wright-Patterson AFB, OH, USA
[b] MRL Materials Resources, LLC, Xenia, OH, USA
[c] Univ. Bordeaux, CNRS, Bordeaux INP, ICMCB, UMR 5026, 33600 Pessac, France

ARTICLE INFO

Keywords:
Refractory complex concentrated alloy
High-temperature strength
Room-temperature ductility

ABSTRACT

Correlations were explored between mechanical, thermodynamic and physical properties of refractory complex concentrated alloys (RCCAs). Experimentally measured yield strengths (σ_y) and ductility were taken from the open literature and were compared against liquidus, solidus and solvus temperatures, elastic properties (Young's, shear and bulk moduli), density (ρ), surface energy (γ) and valence electron concentration (VEC). If not publicly available, the thermodynamic properties were calculated using CALPHAD while the other properties listed above were estimated using a rule-of-mixtures average of the constituent element properties. This analysis emphasized tensile ductility. Based on the identified correlations, useful criteria for selecting possibly ductile RCCA compositions with good high-temperature strength were proposed, a few ductile and strong RCCAs were made and properties of some of them were reported in this paper. Additionally, multivariate linear regression (MLR) was used to identify new insights from the high dimensional space of the present study by modeling the influence of composition and the input thermodynamic and physical properties on the high-temperature strength and room temperature ductility. Equal concentrations of Mo and Nb in RCCAs were found to give a good balance of strength and ductility. The MLR analysis identified over 50 promising RCCAs for intended high-temperature applications, pending experimental confirmation.

1. Introduction

Future aerospace structures require revolutionary new metallic alloys which could operate at very high temperatures, much beyond the currently used Ni-based superalloys [1,2]. Applications include different types of power plants (gas turbine, jet, rocket, nuclear), thermal protection systems and heat exchangers. As motivation, engine thrust and efficiency increase while air pollution decreases with increasing operation (combustion) temperature of power plants [2]. The maximum operating temperatures of Ni superalloys are limited by their relatively low melting temperatures and considerable softening above 1000 °C. For Ni-based superalloys to operate above 1000 °C, special cooling systems are required, which add weight, cost and complexity of the structures.

Refractory complex concentrated alloys (RCCAs) have recently been introduced as promising high-temperature structural alloys [3]. Complex concentrated alloys (CCAs) are defined as alloys consisting of 3 or more principal elements. They are also called multi-principal element alloys (MPEAs) and can have a single phase or multiple phases. CCAs include high entropy alloys, which, by definition, are alloys consisting of 5 or more principal elements, with the concentrations of each element between 5 and 35 atomic % [4]. RCCAs are drawn from a palette of 9 refractory metals (Zr, Hf, V, Nb, Ta, Cr, Mo, W and Re) and they can also contain other elements to optimize properties. The RCCA field opens new composition space and provides huge opportunities for alloy discovery and development. At the same time, the huge composition space is a challenge for timely evaluation of the enormous number of compositions.

Relative to conventional refractory alloys, and even Ni-based superalloys, some RCCAs offer reduced density, improved oxidation and corrosion resistance and superior high temperature (HT) strength [3,5–7]. The density of reported RCCAs ranges from 5.5 to 15 g/cm^3, which covers the density of conventional refractory alloys, nickel alloys and steels, and approaches the density of Ti alloys [8]. The density of RCCAs can be decreased by using lower density refractory elements (Cr, Nb, V and Zr) and low density Al and Ti as principal alloying elements.

* Corresponding author at: Air Force Research Laboratory, Materials and Manufacturing Directorate, Wright-Patterson AFB, OH, USA.
E-mail address: oleg.senkov.ctr@afrl.af.mil (O.N. Senkov).

https://doi.org/10.1016/j.matdes.2024.112762
Received 27 November 2023; Received in revised form 12 January 2024; Accepted 14 February 2024
Available online 16 February 2024

In particular, Cr-Nb-V-Zr-Al-Ti based RCCAs have densities of 5.5–7.0 g/cm^3. Improved oxidation resistance of some RCCAs is thought to be due to formation of complex oxides [3,9]. Due to the variety of compositions, microstructures and phases, RCCAs offer a wide range of mechanical properties, and some of these alloys are considerably stronger than advanced commercial alloys [3]. Because of superior behavior, the interest in the RCCA research area has continuously increased and more than 1000 papers were published by the end of 2022 since the first paper by Senkov et al. [10] in 2010.

In spite of many publications, progress in studying mechanical properties is still limited [3,11,12]. HT mechanical properties are mainly studied in as-cast, powder metallurgy, and/or annealed conditions. Ductile RCCAs are also studied in cold rolled/forged (plus annealed) conditions. Mainly uniaxial compression tests are used during testing above room temperature (RT). Tensile tests are reported only at RT and/or cryogenic temperatures. Only few publications are available on creep [13], fatigue [14,15] and fracture toughness [16–19] of RCCAs. Even with this limited data, a few problems related to strength and ductility of RCCAs are clearly identified. First, it has been recognized that not all RCCAs show high strengths above 1000 °C. Many RCCAs, while being strong at or below 800 °C, rapidly lose their strength between 800 °C and 1000 °C [11]. Second, many RCCAs are found to be brittle at room temperature, which is not acceptable for practical use [12]. Third, it is recognized that the development of an RCCA that is ductile at RT and strong above 1000 °C is a challenge.

In this paper, we attempt to answer the following questions. (i) What materials properties are responsible for HT strength of RCCAs? (ii) Which RCCAs perform better at high temperatures: single-phase or multi-phase? (iii) Is there a correlation between RT and HT strengths? Can RCCAs with HT strength be predicted based on RT testing only? (iv) Why are some RCCAs ductile at room temperature (RT) while others are brittle? Using a thorough analysis of the correlations between RCCA properties, we propose useful criteria for down selection of ductile RCCAs with good high-temperature strength and report compositions and properties of some of these alloys.

2. Methodology

2.1. Mechanical property data sources

RCCA mechanical properties were taken from the databases collected and reported by Gorsse et al. [20], Couzinié et al. [21], Borg et al. [22], Senkov et al. [11,12] and Yurchenko et al. [23], as well as from recent unpublished data collected by the authors. The collected room temperature properties were measured using uniaxial compression or tensile tests, while high-temperature properties were so far reported only from compression tests. Most of the studied alloys were in the as-cast or cast plus annealed conditions, but properties for some alloys were also reported after thermo-mechanical processing. RCCAs made by powder metallurgy were not considered in this study, as contamination with interstitial elements can greatly affect mechanical properties, and the concentrations of interstitial elements were not reported and thus correct correlations of their mechanical properties with the composition and other intrinsic parameters could not be made. The yield stress (σ_y) values were measured as the proof stress at 0.2 % of plastic strain. Compression or tensile ductility was identified as total compression or elongation strain (elastic plus plastic) to fracture. Compression deformation of several reported RCCAs was stopped after 30 %, 40 % or 50 % compression strain with no evidence of fracture. In these cases, compression ductility was assigned to be above the reported amount. To address the possible variability in strength and ductility due to non-optimized microstructure and processing, the upper and lower bounds of ductility vs. yield stress envelopes are emphasized.

2.2. Phase Diagram Calculation

Phase diagrams for the studied alloys were calculated using Thermo-Calc 2021 software and the TCHEA 4.1 database developed by ThermoCalc [24], and Pandat 2020 software and the PanNb 2023 database developed by CompuTherm, LLC [25]. An approach described in detail in an earlier publication [11] was used to assign appropriate liquidus (T_L, the temperature at which solidification starts on cooling), solidus (T_m, the temperature at which solidification completes on cooling) and solvus (T_{solv}, the equilibrium temperature at which the secondary phase starts to precipitate on cooling or completely dissolves on heating) to each of the studied alloys, for which experimental data on these thermodynamic properties are not currently available.

2.3. Rule of mixtures (ROM)

Experimentally reported alloy densities (ρ) and elastic moduli (shear G, Young's E, bulk B) were used or, if not reported, these parameters, as well as valence electron concentration (VEC) and surface energy γ, were calculated using the rule of mixtures, ROM (Equation 1):

$$\rho = \frac{\sum c_i A_i}{\sum c_i V_i} \tag{1a}$$

$$G = \frac{\sum c_i V_i G_i}{\sum c_i V_i};\ E = \frac{\sum c_i V_i E_i}{\sum c_i V_i};\ B = \frac{\sum c_i V_i B_i}{\sum c_i V_i} \tag{1b}$$

$$\gamma = \frac{\sum c_i V_i \gamma_i}{\sum c_i V_i} \tag{1c}$$

$$VEC = \frac{\sum c_i (VEC)_i}{\sum c_i} \tag{1d}$$

Here c_i, A_i, V_i, G_i, E_i, B_i and γ_i are, respectively, the atom fraction, molar mass, molar volume, shear modulus, Young's modulus, bulk modulus and surface energy of element i at room temperature (RT). The ROM values, except VEC, can be applied to 1-phase RCCAs only. ROM values cannot be applied to multi-phase (M-phase) RCCAs because different phases have different chemical compositions and some of them can be ordered. ROM-calculated VEC can be used for M-phase RCCAs in the temperature ranges where these alloys become single-phase structures, as VEC is a temperature-independent parameter. It was shown earlier that the values of the elastic moduli of single-phase (1-phase) RCCAs calculated using first principles and the rule of mixtures are very similar [3,26–29]. The surface energy of binary solid solutions also follow this rule [30], although no information is yet available if a ROM can be used to calculate surface energy of 1-phase RCCAs.

2.4. Modeling and predicting alloy properties

Multivariate linear regression (MLR) [31] was used to quantify the effect of alloy composition on the strain at room temperature and σ_y at elevated temperatures. MLR is well adapted for this task, since it minimizes the risk of overfitting when applied to datasets with many features but relatively few observations. MLR gives an interpretable first-order approximation that allows the relative contributions of input parameters on the predicted properties to be estimated. The model exclusively used compositional features, considering the practicality of this approach for alloy design and the direct correlation it offers between the alloy composition and its mechanical properties. Outliers in mechanical properties were removed to prevent the model from being overly influenced by extreme data points. Outliers were determined by their position beyond 1.5 times the interquartile range (IQR = Q3-Q1), either below the first quartile (Q1) or above the third quartile (Q3), in accordance with the standard outlier detection method. To avoid complexities associated with microstructural variations, the MLR training was restricted to 1-phase RCCAs. Fewer than 10 alloys in the datasets contain

Re or Si, so these elements were excluded from statistical MLR analyses.

To evaluate the robustness and generalizability of the MLR predictive model, we employed Leave-One-Out Cross Validation (LOOCV). In this technique, each observation in the original sample is used once as the validation data, with the remaining observations serving as the training data. Through LOOCV, we calculated key performance metrics that quantify the model's accuracy and predictive power: Mean Squared Error (MSE), Mean Absolute Error (MAE), and the coefficient of determination (R^2).

The available data were organized into two separate datasets to support the statistical modeling in this study, one for HT properties measured using uniaxial compression tests and the other for RT properties measured in tension and compression. The first dataset includes 44 1-phase and 24 M-phase RCCAs, and the second dataset contained 69 1-phase and 42 M-phase RCCAs, as well as a few conventional refractory alloys.

3. Data exploration and analysis

3.1. Overview of correlations in RCCA properties

A statistical view of the RCCA compositions used in this analysis is shown in Fig. 1, illustrating the frequency and distribution of elemental constituents in the two RCCA datasets for elevated temperature compressive σ_y and room temperature properties. The bar charts at the top of each panel show the frequency of occurrence for each element in the datasets, highlighting the prevalence of Nb, Ti, and Zr. The boxplots below the bar charts show the concentration ranges of the elements within the alloys, with the red line in each box indicating the median value and the green line representing the mean. The interquartile range captures the middle 50 % of data points, and whiskers extend from the quartiles to the furthest data points within 1.5 times the interquartile range, indicating the overall spread, while points outside this range are marked as outliers with discrete dots.

It is generally thought that M-phase RCCAs can be stronger than 1-phase RCCAs because of an additional contribution from precipitation strengthening. To see how much the secondary phases actually contribute to the strength of RCCAs, the data were analyzed in two groups: 1-phase and M-phase RCCAs.

Fig. 2 gives a panoramic view of the relationships between RCCA constituent elements and properties. Included properties include solvus, solidus and liquidus temperatures obtained via CALPHAD; ρ, VEC, and G approximated by the rule of mixtures; and experimentally measured σ_y and total compressive strain from RT to 1200 °C. This heatmap shows the presence and the strength of correlations using Pearson's correlation coefficient (r). A strong correlation is indicated when $0.7 < |r| \leq 1$, a moderate correlation occurs for $0.3 \leq |r| \leq 0.7$, and $0 \leq |r| < 0.3$ shows a weak correlation or no relationship. A positive correlation occurs for positive r values, indicating that an increase in the input parameter is associated with an increase in the material property. Negative r values produce a negative correlation, where an increase in the input value produces a decrease in the correlated property, and vice versa. Care is needed in interpreting correlation heat maps, since false correlations can be produced by limited sample sizes. For example, false correlations are essentially absent when analyzing 1000 observations in a 10-dimensional composition space with 10 features, false correlations of small-to-moderate intensity can be present when analyzing only 50 observations (similar to the datasets used here), and false correlations can be moderate-to-strong when only 10 observations are available for correlation.

The heatmap in Fig. 2 is divided into two segments - the upper right shows results for 1-phase and the lower left for M-phase RCCAs. Clear differences in correlation coefficients between 1-phase and M-phase RCCAs emphasize the significant impact of microstructure on alloy properties. The data show that T_L is a critical indicator of mechanical strength. In M-phase RCCAs, T_L has a strong positive correlation with HT strength and a moderate influence on strength at 800 °C and RT. T_{solvus} has a slightly lower correlation with strength, and T_m is the least

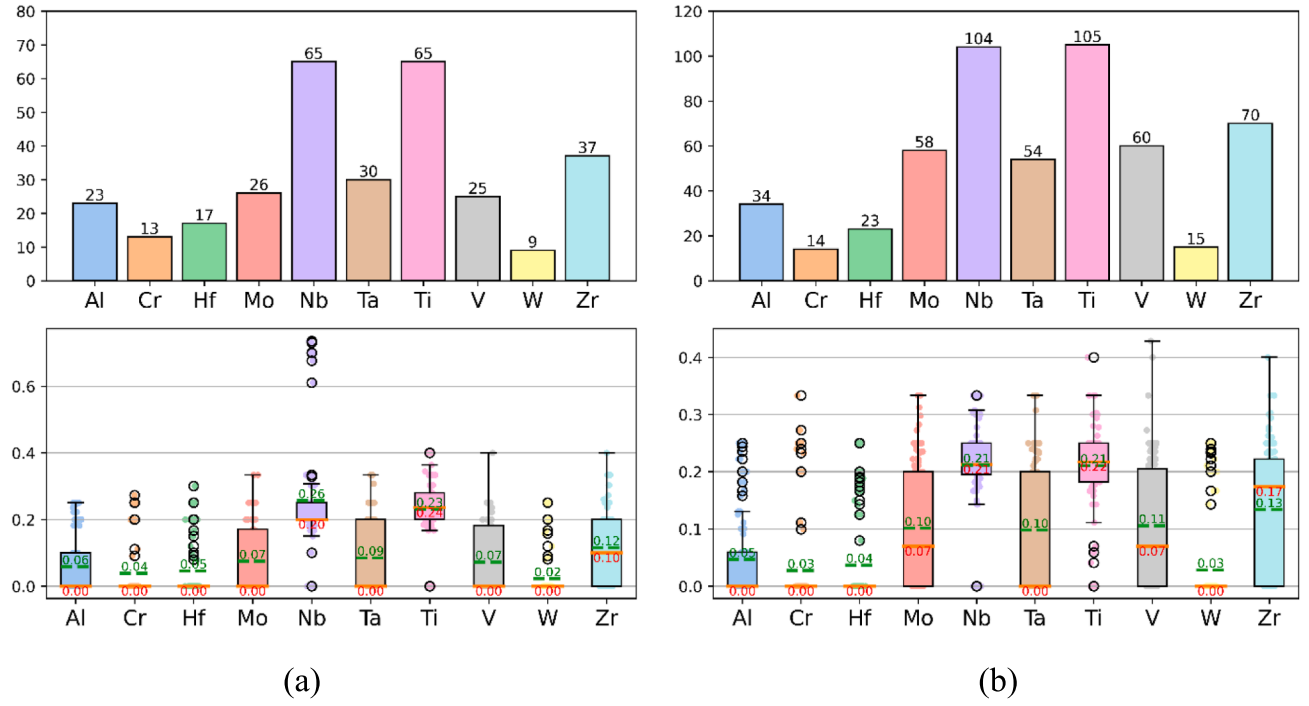

Fig. 1. Elemental profiles of the RCCA datasets in this study for (a) alloys used to measure σ_y in compression at elevated temperature, and (b) alloys used to measure RT strength and ductility. The bar charts in the upper panels show the number of alloys that contain each respective element, and the boxplots in the lower panels reveal the concentration distribution for each element. The interquartile ranges (IQR = Q3-Q1) are shown by the boxes, with median values marked by red lines across the boxes and mean values by green dashed lines. Outliers are represented as individual points. (For interpretation of the references to color in this figure legend, the reader is referred to the web version of this article.)

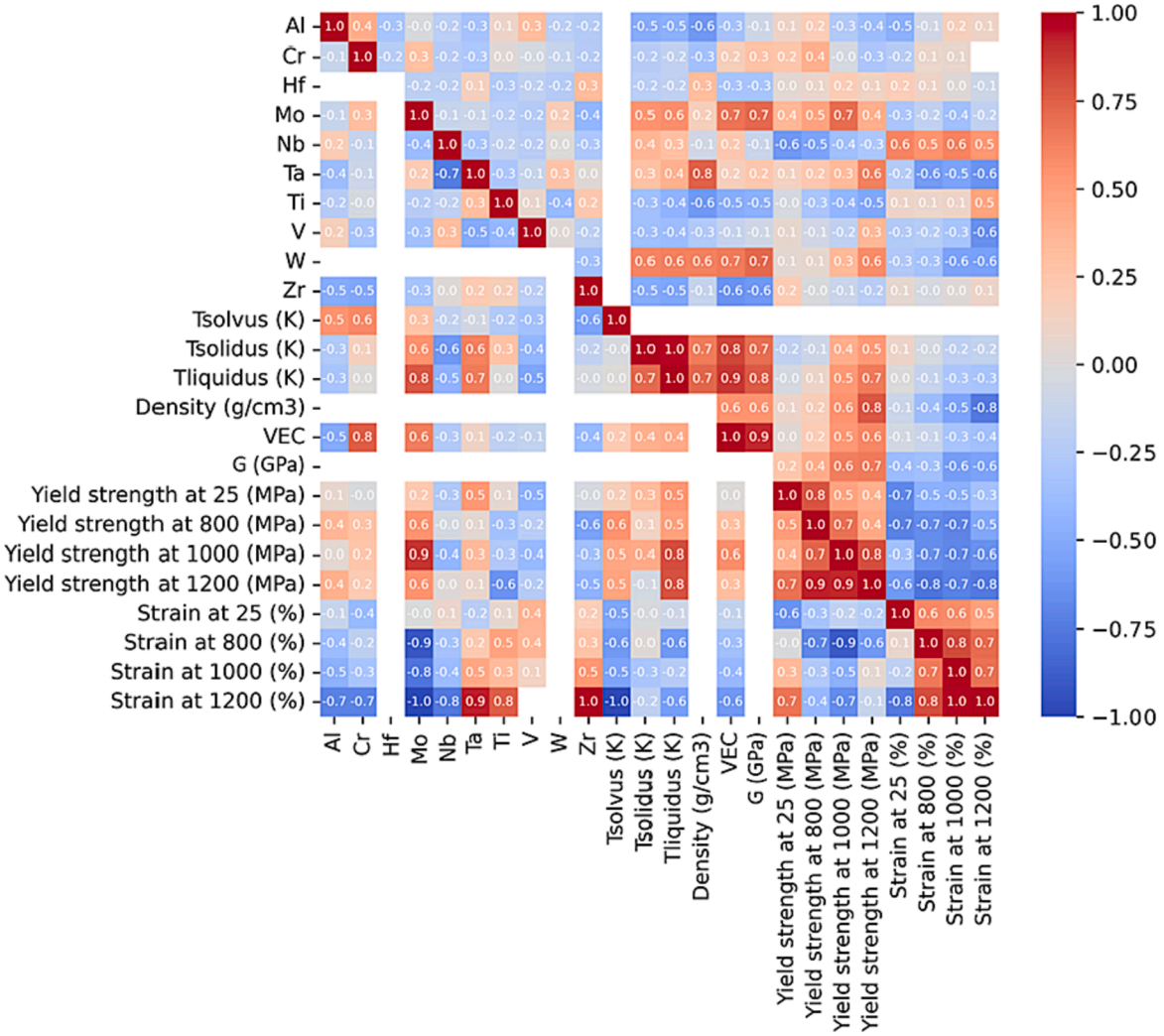

Fig. 2. 'Heatmap' showing correlations between alloy parameters and mechanical properties for 1-phase (upper right) and M-phase (lower left) RCCAs. Each cell includes the value of the corresponding Pearson correlation coefficient (r), and is color-coded from blue (negative correlation with $-1 \leq r \leq 0$) to red (positive correlation with $0 \leq r \leq 1$). Density and shear modulus (G) values derived from the ROM are excluded for M-phase RCCAs. (For interpretation of the references to color in this figure legend, the reader is referred to the web version of this article.)

significant of the thermodynamic temperatures. For 1-phase RCCAs, there is a strong-to-moderate positive correlation between T_L and HT strength but essentially no correlation with σ_y at RT. T_m shows a moderate influence on HT σ_y. The heatmap's red gradient signals a strong positive correlation between G, VEC, ρ, and σ_y at elevated temperatures for 1-phase RCCAs. The positive correlation between VEC and high-temperature yield strength is also observed for M-phase RCCAs, while a moderate-to-weak tendency for ductility to decrease with increasing VEC is noted for both types of RCCAs (Fig. 2).

Fig. 3 focuses on the relationships between RT strength and ductility and appropriate input parameters. In 1-phase RCCAs, the RT σ_y shows the strongest positive correlation with G/B ($r = 0.4$) and the presence of Mo ($r = 0.5$), while RT ductility is most closely dependent on G, E, G/B and Gb/γ (b is the Burgers vector), all with $r = -0.6$, and on the use of Mo ($r = -0.5$). The correlation heatmap for M-phase RCCAs excludes values determined by the ROM, and so RT properties were only correlated with constituent elements. Correlations between the other alloying elements and RT properties were usually weak. The strongest positive correlations were between RT strength and the use of W (0.4) and Ta (0.3), and negative correlations were found with Nb (−0.5) and Zr (−0.3). For RT tensile ductility, the most notable correlations were with Zr (0.4) and Cr (−0.4).

Transitioning from the broad correlations presented in Figs. 2 and 3, the following sections explore the details of these relationships. Sections 3.2 and 3.3 examine the influence of thermal properties, ρ and VEC on elevated temperature properties, and Section 3.4 discusses the interplay between these material properties and the RT tensile ductility of RCCAs.

3.2. *Effects of composition and thermodynamic parameters on RCCA strengths*

Fig. 4a and b show the temperature dependence of σ_y for the two groups, 1-phase and M-phase, of RCCAs. Additionally, the temperature dependence of refractory metals, conventional refractory alloys and two representative Ni-based superalloys are shown in Fig. 4c. As a reference point, a suggested lower bound of 300 MPa for the HT (1200 °C) yield stress is also shown in the figures as a dashed horizontal line. It can be seen that M-phase RCCAs are stronger than 1-phase RCCAs at temperatures below 600–800 °C, likely due to additional precipitation strengthening. However, the strength of M-phase RCCAs decreases rapidly between 600 and 1200 °C, due to dissolution of secondary phases and loss of the precipitation strengthening effect, and at 1200 °C none of them have yield stresses above the 300 MPa target. On the contrary, the yield stress of 1-phase RCCAs is less temperature dependent and many 1-phase RCCAs retain higher strengths than M-phase RCCAs above 900–1000 °C. In comparison, the temperature dependence

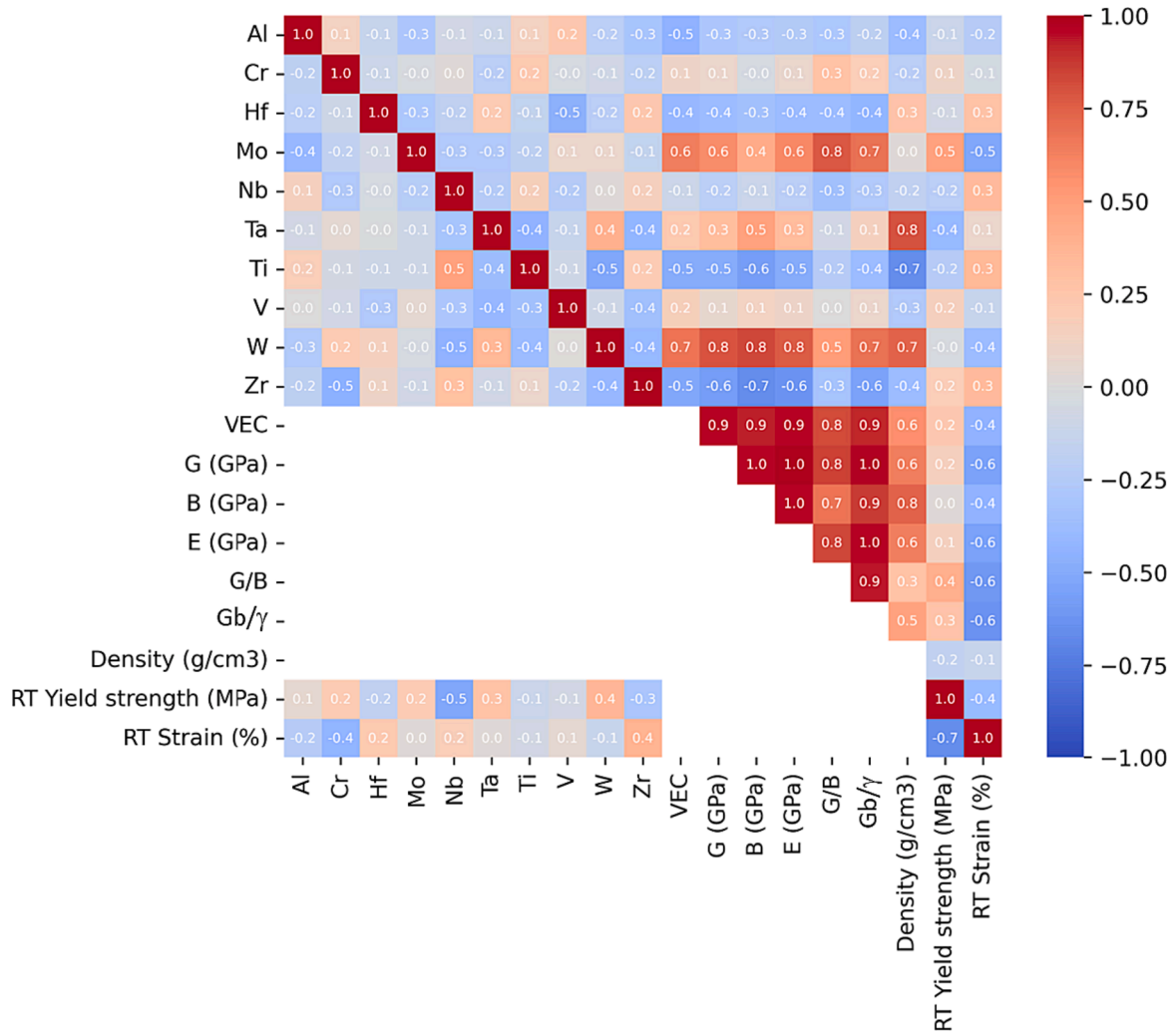

Fig. 3. 'Heatmap' showing correlations between alloy parameters and RT properties for 1-phase (upper right) and M-phase (lower left) RCCAs. Each cell includes the value of the corresponding Pearson correlation coefficient (r), and is color-coded from blue (negative correlation with $-1 \le r \le 0$) to red (positive correlation with $0 \le r \le 1$). Values derived from the ROM are excluded for M-phase RCCAs. (For interpretation of the references to color in this figure legend, the reader is referred to the web version of this article.)

of σ_y for representative refractory metals and conventional alloys, which all have predominantly 1-phase structure, is also weak, but these materials are overall softer than 1-phase RCCAs, likely due to a smaller solid solution strengthening effect. The behavior of Ni-based superalloys, which are multi-phase structures, is similar to the behavior of M-phase RCCAs (Fig. 4c).

When the absolute testing temperature T is normalized by T_L for each of the studied alloys, the HT stress drop is observed in all RCCAs within almost the same homologous temperature range, $T/T_L \sim 0.5–0.6$ (Fig. 5 a, b). This shows that RCCAs with higher T_L can keep their strength to higher temperatures. Interestingly, the stress drop in commercial refractory alloys also occurs at $T \sim 0.5–0.6\ T_L$, while in Ni-based superalloys it occurs at slightly higher T/T_L, ~0.55–0.70 (Fig. 5c). The higher homologous temperatures associated with the decrease in superalloy yield strength are likely due to the exquisite control of microstructure and to the anomalous yield strength behavior for the intermetallic Ni_3Al compound.

To verify the effect of T_L on yield stress, the yield stresses of different RCCAs tested at RT and 1200 °C were plotted against liquidus temperatures of these alloys (Fig. 6). No effect of T_L on RT yield stress was found (Fig. 6a). However, there is a strong tendency for the HT yield stress to increase with increasing T_L (Fig. 6b). Among the reported RCCAs, those having higher T_L generally have higher yield stress at 1200 °C and all RCCAs with yield stress above 300 MPa at 1200 °C have T_L above 2100 °C.

At the same T_L, M-phase RCCAs are stronger than 1-phase RCCAs at RT (Fig. 6a). However, many 1-phase RCCAs are stronger than M-phase RCCAs above 1000 °C due to their higher T_L (Fig. 4, Fig. 6). In fact, the 1200 °C yield strengths of reported M-phase RCCAs do not exceed 300 MPa, while those of many 1-phase RCCAs are much above 300 MPa (Fig. 6b). In addition to low T_L, the noticeable strength drop of M-phase RCCAs at 0.5–0.6 T_L can also be related to the dissolution of second-phase particles (low T_{solv}) and the loss of precipitation strengthening [11]. These correlations suggest the development of M-phase RCCAs with $T_L > 2100$ °C and with second-phase strengthening particles that remain stable above the intended use temperature.

Fig. 7 shows correlations between RT yield stress and HT (1000 °C and 1200 °C) yield stress values for 1-phase RCCAs. When all the RCCAs are considered, no correlation between RT and HT yield stresses is observed (Fig. 7a). However, when the alloys are divided in two groups, one group having the absolute homologous testing temperature $T/T_L < 0.55$, and the second group having $T/T_L \ge 0.55$, a strong correlation between RT and HT stresses is found for the first group (Fig. 7b) and no correlation for the second group (Fig. 7c). These findings may indicate that the same strengthening mechanism operates at $T < 0.55\ T_L$ and thus in this temperature range the HT strength can be roughly predicted from

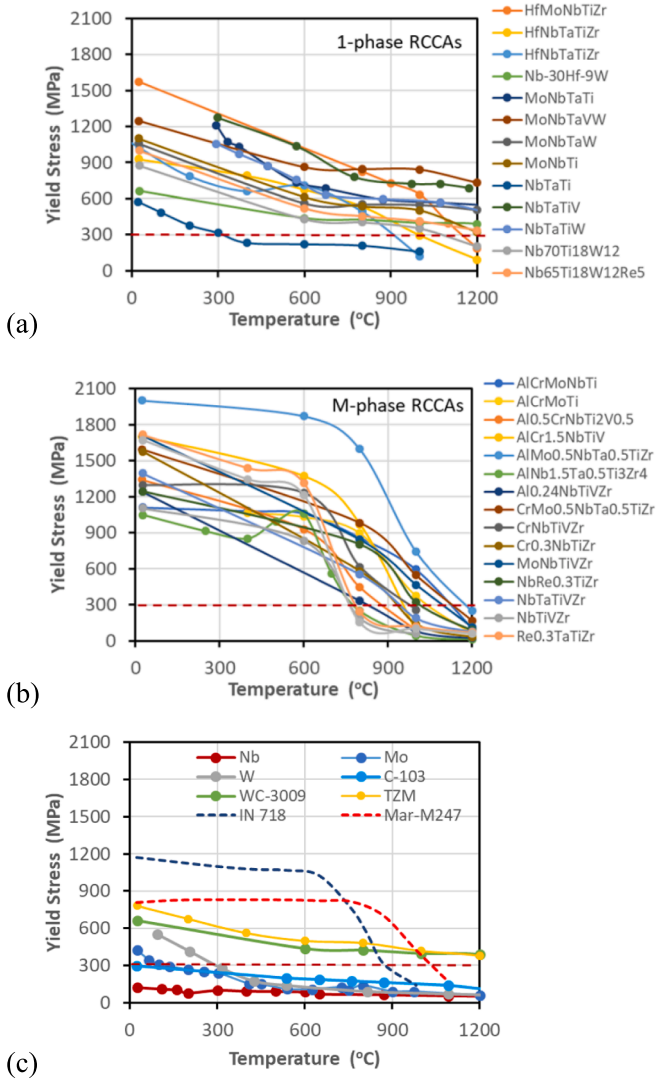

Fig. 4. Temperature dependence of yield stress for (a) single-phase BCC RCCAs, (b) multi-phase RCCAs and (c) three pure refractory metals (Mo, Nb, W), three conventional refractory alloys (C-103, WC-3009, TZM) and two Ni-based superalloys (IN 718 and Mar-M 247).

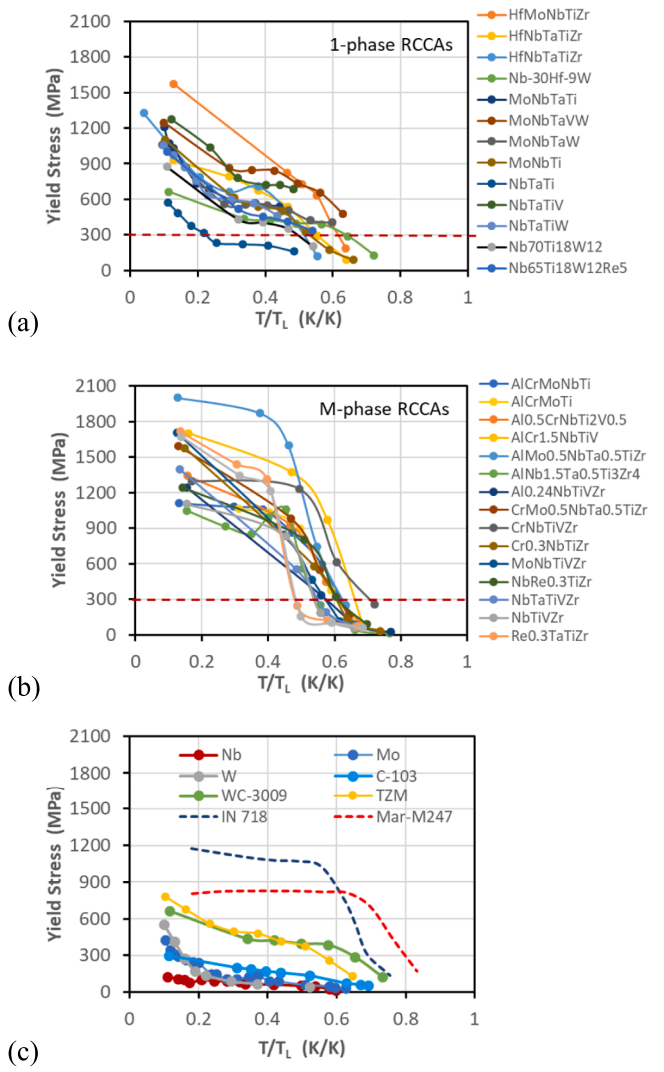

Fig. 5. Dependence of yield stress of (a) 1-phase RCCAs, (b) M-phase RCCAs and (c) representative refractory metals, refractory conventional alloys and Ni-based superalloys on the homologous temperature, T/T$_L$.

RT measurements. For example, the Maresca-Curtin strengthening model based on edge dislocation mobility predicts a direct correlation between the room temperature and HT strength [33]:

$$\sigma_y^T = \sigma_y^{300K} \frac{\left(1-(\alpha T)^{2/3}\right)}{\left(1-(300\alpha)^{2/3}\right)} \tag{2}$$

where σ_y^{300K} and σ_y^T are the yield stresses at 300 K and T, where T is the testing temperature (in K) and α is a material constant. On the other hand, strengthening mechanisms operating above 0.55 T$_L$ are likely different from those operating at lower temperatures, and the HT properties cannot be predicted from the low-temperature measurements. Indeed, the Rao-Suzuki model of screw dislocation solid solution strengthening for 1-phase BCC RCCAs considers different strengthening mechanisms for low-temperature (diffusionless dipole dragging) and HT (diffusion-controlled jog dragging) regimes [34]. This approach predicts a steep drop in yield stress in the temperature range of 0.55–0.6T$_L$, where the transition from one to the other mechanism occurs, in agreement with the experimental data shown in this study.

3.3. *Effect of alloy density and valence electron concentration on high-temperature strength of RCCAs*

There is a general trend for refractory metals with higher melting points to have higher densities. A similar trend is also present for RCCAs (Fig. 8a). Their density increases almost linearly with increasing T$_L$. Therefore, one can expect that RCCAs having high strength at high temperatures have both high T$_L$ and high ρ. Indeed, when 1200 °C yield stress is plotted versus the density of the reported RCCAs, a trend can be seen that the yield stress increases with increasing alloy density (Fig. 8b). All the reported RCCAs, but one (MoTiZr), with 1200 °C yield stress above 300 MPa have densities above 8 g/cm^3 and those with yield stress above 400 MPa have density above 8.9 g/cm^3 (Fig. 8b). On the other hand, all low density RCCAs (ρ ≤ 7.5 g/cm^3) are soft at 1200 °C. Fortunately, the specific yield stress (yield stress divided by the alloy density) also has a tendency to increase with increasing alloy density (Fig. 8c). This analysis indicates that RCCAs with high strength and high specific strength at high temperatures (≥1200 °C) will also have high density, above 8–9 g/cm^3. Low density RCCAs, which have been developed recently aiming to increase the specific strength, have low T$_L$ and lose their strength and specific strength above 1000 °C.

Fig. 8d shows that HT strength of RCCAs has a tendency to increase

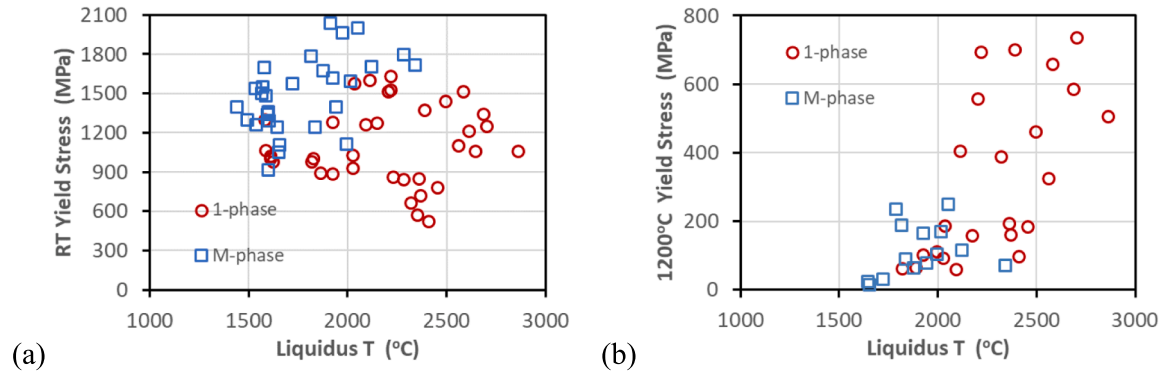

Fig. 6. Effect of the liquidus temperature on (a) room temperature (RT) and (b) 1200 °C yield stress of RCCAs.

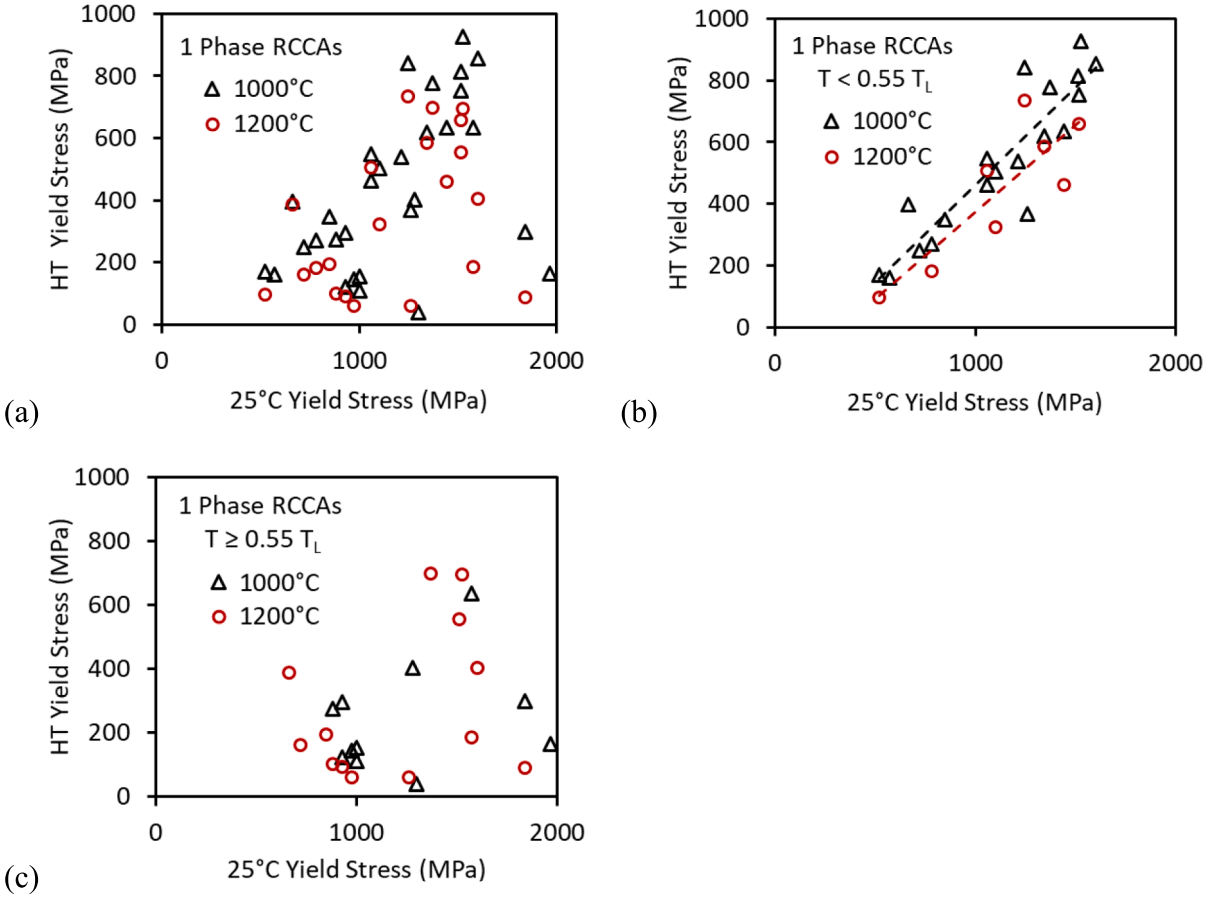

Fig. 7. Correlations between room temperature (25 °C) and high temperature (1000 °C and 1200 °C) yield stresses for (a) all analyzed RCCAs, (b) RCCAs for which the testing temperatures are below 0.55 T_L, and (c) RCCAs for which the high-temperature testing temperatures are above 0.55 T_L.

when the valence electron concentration (VEC) of an alloy increases from 4 to 6. Combining this observation with the positive effect of T_L and ρ, one can suggest that RCCAs with high strengths above 1000 °C should be rich in Nb, Ta, Mo and/or W. These elements are commonly used in RCCAs (Fig. 1). All RCCAs with yield strengths above 300 MPa at 1200 °C have VEC > 4.6. However, a number of RCCAs that meet this criterion have yield strengths that are below the 300 MPa threshold at 1200 °C, so this is a necessary, but not sufficient, phenomenological condition. The more stringent criterion of VEC > 5.1 is a sufficient condition for yield strengths exceeding 300 MPa at 1200 °C with the current dataset.

Table 1 shows nine reported RCCAs with yield stress above 400 MPa at 1200 °C. They all have $T_L > 2100$ °C, $\rho \geq 8.9$ g/cm^3 and VEC ≥ 4.6. All alloys contain Mo and five contain W, and all are 1-phase structures. The properties for these alloys were reported in cast or cast plus HIP conditions using compression tests. None of these alloys were tested in tension.

3.4. RCCA tensile ductility

The matrix phase of the currently reported RCCAs have a BCC crystal structure and, as all BCC materials, these RCCAs experience a brittle-to-ductile transition and become brittle below a critical temperature T_{DBT}. For practical use, T_{DBT} of an alloy should generally be below room

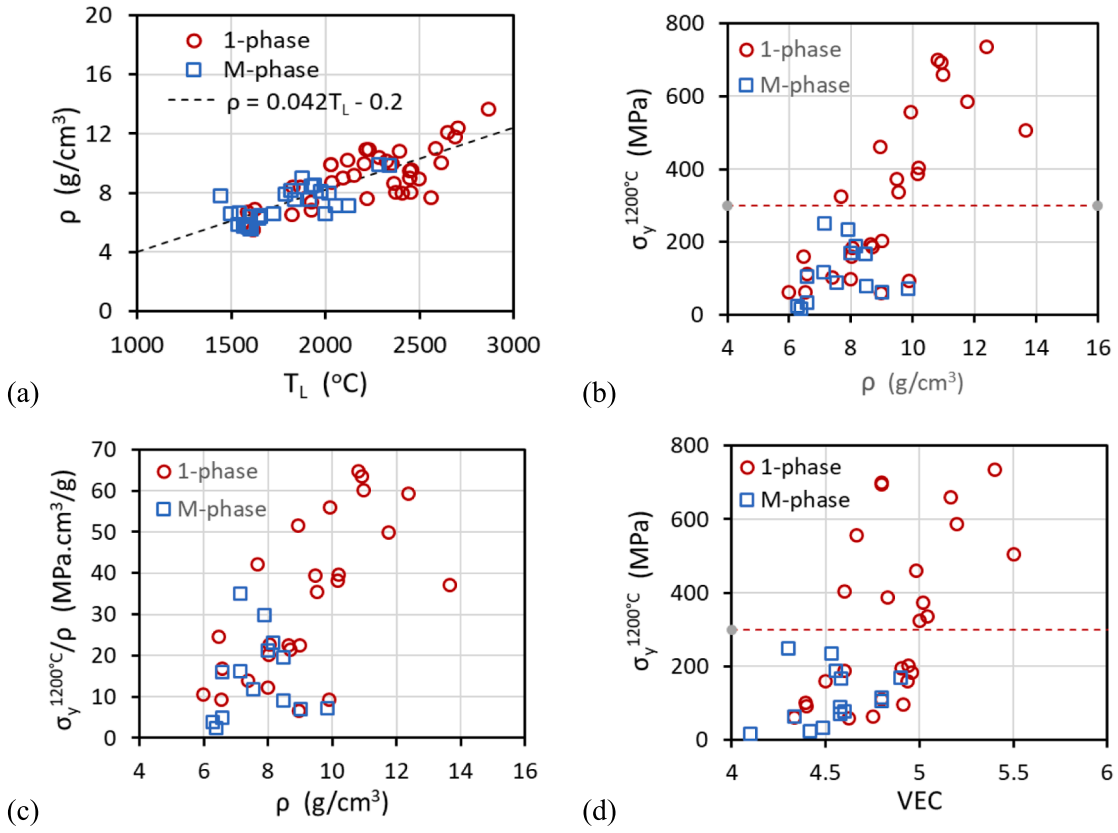

Fig. 8. Correlations between (a) alloy density (ρ) and liquidus temperature (T_L), (b) 1200 °C yield stress ($\sigma_y^{1200°C}$) and density (ρ), (c) 1200 °C specific yield stress ($\sigma_y^{1200°C}/\rho$) and density (ρ) and (d) 1200 °C yield stress and valence electron concentration (VEC) of reported RCCAs.

Table 1
Nine reported RCCAs with yield stress above 400 MPa at 1200 °C.

Alloy ID	ρ (g/cm³)	T_m (°C)	T_L (°C)	$\sigma_y^{1200°C}$(MPa)	$\varepsilon_f^{1200°C}$(%)	$\sigma_y^{25°C}$(MPa)	$\varepsilon_f^{25°C}$(%)	VEC	Refs
HfMoNbTaTi	10.8	2145	2390	699	>30	1369	27	4.8	[35]
HfMoNbTaTiZr	9.9	1890	2205	556	>30	1512	12	4.67	[35]
HfMoNbTaZr	10.9	1912	2218	694	>30	1524	16	4.8	[35]
HfMoTaTiZr	10.2	1825	2114	404	>30	1600	4	4.60	[35]
MoNbTaTiVW	11.0	2417	2584	659	8	1515	11	5.17	[36]
MoNbTaTiW	11.8	2607	2689	586	10	1343	14	5.20	[36]
MoNbTaVW	12.4	2566	2704	735	8	1246	2	5.40	[37]
MoNbTaW	13.7	2804	2864	506	>40	1058	6	5.50	[37]
$Mo_{17}Nb_{33}Ti_{34}W_{16}$	8.9	2434	2496	461	>50	1440	11	4.98	[38]

temperature. Therefore, we analyzed the RT ductility of reported RCCAs. A similar analysis was conducted earlier, but fewer RCCAs were available at that time [12]. While RT testing of RCCAs continues to emphasize compressive loading, a growing number of tensile studies are reported. Therefore, here we analyze the tensile data that are now available. Fig. 9 shows RT tensile ductility (total strain to failure) as a function of tensile yield stress (σ_y) and valence electron concentration (VEC) for a number of RCCAs and conventional refractory alloys (CRAs). The properties of 79 1-phase RCCAs, 9 M-phase RCCAs, 18 RCCAs experiencing phase transformations during tensile testing (transformation-induced plasticity, TRIP) and 7 CRAs are given in the as-cast condition (95 data points, all RCCAs) and thermo-mechanically processed (TMP) conditions (92 data points, including 11 for CRAs). It can be seen that, depending on the composition and TMP, the tensile ductility of RCCAs varies from 0 % to up to 50 %. All TRIP, many 1-phase and some M-phase RCCAs have good RT tensile ductility, which generally increases after TMP [23]. Tensile ductility tends to decrease with increasing σ_y (Fig. 9a). All RCCAs with σ_y below 800 MPa are ductile and between 800 and 1600 MPa can be ductile or brittle. There are no tensile data for RCCAs with yield stress exceeding 1600 MPa, which may indicate that the RCCAs with yield stress above 1600 MPa are likely brittle [12]. There is no effect of VEC on RT tensile ductility for VEC from 4.0 to 5.1 (Fig. 9b): at the same VEC values in this range, some RCCAs can be ductile and others brittle. It can also be noted that all TRIP RCCAs have VEC below 4.2 and, therefore, these RCCAs are expected to be soft above 1000 °C (see Section 3.2).

Fig. 10 shows the dependence of tensile elongation on (a) shear modulus G reduced by bulk modulus B (G/B) and (b) dislocation line tension energy (Gb) reduced by the surface energy γ (Gb/γ) for the reported single-phase RCCAs and CRAs. Here $b = \sqrt{3}a/2$ is the magnitude of the Burgers vector, which average value of 0.29 nm was estimated from the reported lattice parameters a of 1-phase BCC RCCAs and used in the current work. According to the Pugh-Pettifor ductility criterion, an alloy is incipiently ductile if $G/B < 0.4$–0.6 [39]. According to the Rice-Thomson criterion, an alloy is incipiently ductile if $Gb/\gamma < 7.5$–10 [40]. Analysis of the experimental data indicates that all reported 1-

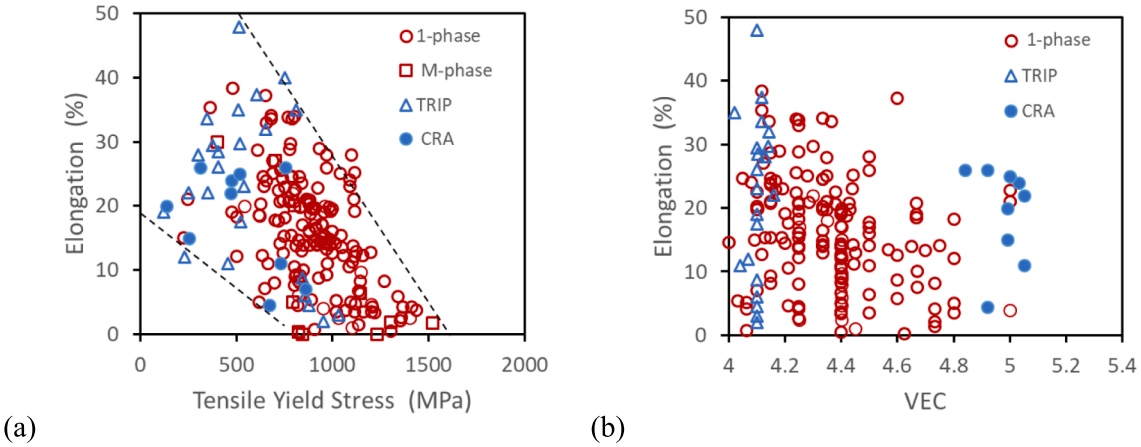

Fig. 9. Room temperature elongation to failure of RCCAs and conventional refractory alloys (CRAs) as a function of (a) tensile yield stress and (b) valence electron concentration. The RCCAs are divided into three groups: single-phase (1-phase), multi-phase (M-phase) RCCAs, as well as of RCCAs experiencing a phase transformation during testing (TRIP).

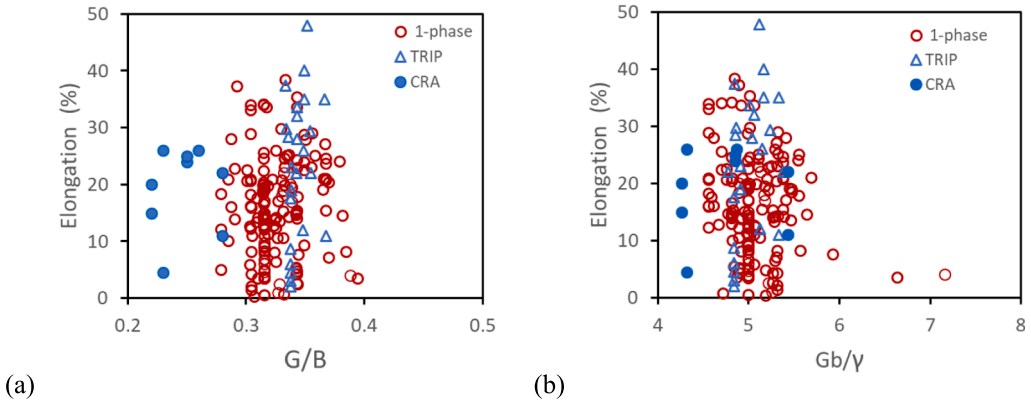

Fig. 10. Tensile ductility of RCCAs and CRAs as a function of (a) G/B and Gb/γ, where G, B, b and γ are the shear modulus, bulk modulus, the magnitude of the Burgers vector and surface energy of an alloy, respectively.

phase RCCAs are incipiently ductile, in accord to these two criteria. Thus, the observed brittleness of some of them is likely due to extrinsic effects such as defects present after casting and/or processing or interstitial segregation to grain boundaries, which can lead to premature grain boundary decohesion. Brittle failure may also occur in BCC alloys when the yield strength is higher than the intrinsic fracture stress of the material. As a result, RCCAs with very high RT yield strengths may fail by transgranular cleavage before the stress needed to move dislocations is reached. This can serve as a dis-incentive to seek exceptional RT yield strengths in RCCAs intended for HT use.

Earlier, Sheikh et al. [41], based on limited experimental data at that time, proposed a VEC ductility criterion according to which ductile RCCAs have VEC < 4.5–4.6 and RCCAs with VEC > 4.6 are brittle. The current analysis indicates that this criterion needs to be revised, as both

Table 2
List of RCCAs which are ductile at room temperature and satisfy the criteria for high-temperature strength.

Alloy	Condition	$\sigma_y^{25^\circ C}$ MPa	$\varepsilon_f^{25^\circ C}$%	VEC	T_L°C	ρ g/cm^3	σ_y^{HT} MPa	Refs
$Hf_5Nb_{55}Ta_{25}Ti_{15}$	TMP	750	1.0	4.80	2435	10.3	N/A [a]	[42]
$Hf_5Nb_{55}Ta_{25}Ti_{15}$	TMP	500	18.3	4.80	2435	10.3	N/A [a]	[42]
$Hf_5Nb_{55}Ta_{25}Ti_{15}$	TMP	500	12.1	4.80	2435	10.3	N/A [a]	[42]
$Hf_5Nb_{55}Ta_{25}Ti_{15}$	TMP	620	5.0	4.80	2435	10.3	N/A [a]	[42]
HfNbTa	as-cast	847	10.0	4.67	2416	12.9	N/A [a]	[43]
HfNbTa	TMP	871	20.8	4.67	2416	12.9	N/A [a]	[43]
$Nb_{35}Ta_{35}Ti_{15}Zr_{15}$	as-cast	970	13.3	4.70	2323	10.3	102 (1200 °C)	[44]
$NbSi_{0.1}TaTiV$	as-cast	1135	1.4	4.73	2093	9.0	N/A [a]	[45]
$NbSi_{0.1}TaTiV$	TMP	1355	2.1	4.73	2093	9.0	N/A [a]	[45]
$NbSi_{0.1}TaTiV$	TMP	1413	4.2	4.73	2093	9.0	N/A [a]	[45]
$NbSi_{0.1}TaTiV$	TMP	1270	8.2	4.73	2093	9.0	N/A [a]	[45]
NbTaTi	as-cast	620	18.5	4.67	2342	10.0	160 (1000 °C)	[46]
NbTaTiV	as-cast	727	14.1	4.75	2144	9.2	688 (900 °C)	[45]
NbTaV	as-cast	925	22.8	5.00	2393	10.8	N/A [a]	[47]
TaTiV	TMP	801	7.6	4.67	2083	9.4	N/A [a]	[48]

(a) Not available.

brittle and ductile alloys can have any VEC value in the range of VEC from 4 to 5 (Fig. 9b).

Among the studied RCCAs which showed RT tensile ductility, only 8 satisfy the criteria suggested earlier in this manuscript for HT strength ($T_L > 2100$ °C; VEC > 4.6; $\rho > 8$ g/cm^3). The compositions, conditions (as-cast or TMP) and properties of these alloys are shown in Table 2. For RCCAs where data are available in both the as-cast condition and after TMP, it can be seen that RT tensile ductility of these alloys is higher after TMP. None of the alloys contain Mo or W and their high density is due to the presence of Hf or Ta, or both of these elements. Only three of these compositions have reported properties at elevated temperatures, which were measured during compression testing. Among these three, $Nb_{35}Ta_{35}Ti_{15}Zr_{15}$ and NbTaTi, are soft at T ≥ 1000 °C. This could be due to low values of solute-screw dislocation interaction energies in these alloys [34]. The third alloy, NbTaTiV has a yield stress of 688 MPa at 900 °C, but no data is available at higher temperatures.

3.5. Multivariate linear regression predictive model outputs and evaluation

Fig. 11 shows the predictive accuracy of the MLR models. Fig. 11a compares the actual σ_y at 1000 °C with values predicted by the MLR models trained on the datasets in this study. Each datapoint corresponds to an alloy, giving actual (*x*-axis) and predicted (*y*-axis) σ_y values. The dashed line indicates perfect agreement, and the coefficient of determination ($R^2 = 0.73$) shows overall reliable predictions. As a strong effect of Mo on the studied properties was found and all the reported RCCAs contain Nb, the data-points in Fig. 11 are color-coded to indicate the atom fraction difference between Mo and Nb, with a red shift for positive differences ($c_{Mo} > c_{Nb}$) and a blue shift for negative differences ($c_{Mo} < c_{Nb}$). This shows that the strongest alloys at 1000 °C – those with $\sigma_y > 500$ MPa – all have more Mo than Nb. A similar comparison plot is shown for σ_y at 1200 °C (Fig. 11b). The MLR model accuracy is similar ($R^2 = 0.74$), but RCCAs with more Mo than Nb now span the range from low to high σ_y values. The MLR model shows an improved predictive

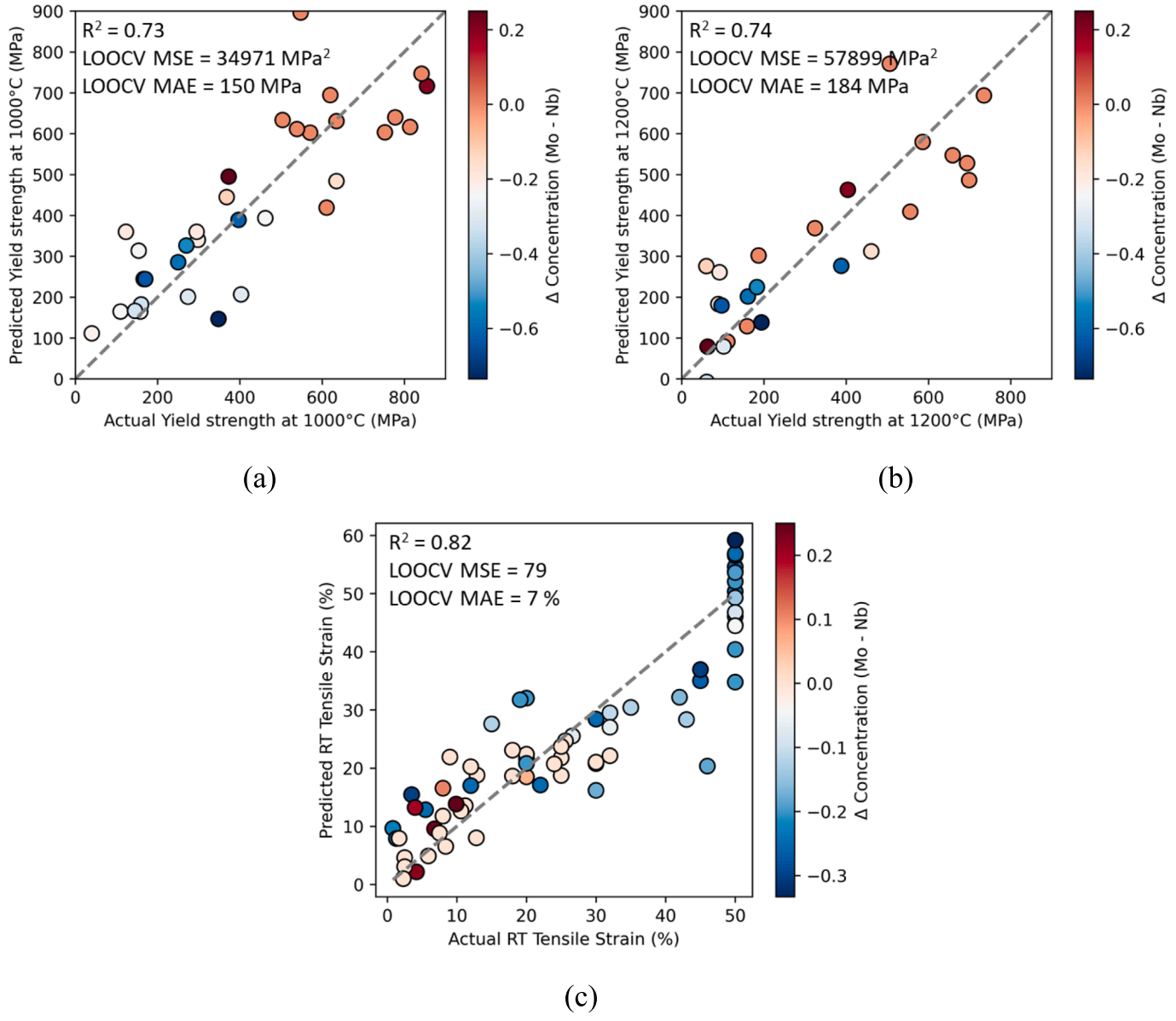

Fig. 11. Multivariate linear regression (MLR) model accuracy in predicting 1-phase RCCA (a) σ_y at 1000 °C, (b) σ_y at 1200 °C, and (c) total RT strain to failure. Each datapoint represents an RCCA, and datapoints are color-coded to show the difference in atom fraction between Mo and Nb, $c_{Mo} - c_{Nb}$. The coefficient of determination (R2), mean squared error (MSE) and mean absolute error (MSE) determined by leave-one-out cross validation are also provided.

capability for total RT strain (Fig. 11c), with $R^2 = 0.82$. Here, all but two RCCAs with total strains ≥30 % have more Nb than Mo. While most RCCAs with total plasticity <30 % have more Mo than Nb, many also show the opposite trend.

Collectively, these plots demonstrate a good effectiveness of the MLR model, offering predictions that align reasonably well with actual values and providing a means to navigate the compositional landscape and predict mechanical properties of RCCAs in unseen regions.

Fig. 12 shows the influence of individual constituent elements on the predicted mechanical properties of RCCAs. The HT strength is most positively affected by the presence of Mo, W, Hf, and Ta and is negatively correlated with Ti, Cr and Nb alloying additions (Fig. 12a,b). Other elements have a mixed influence. V negatively affects σ_y at 1000 °C yet positively at 1200 °C. Both Al and Zr exhibit minimal impact on 1000 °C strength but reduce strength at 1200 °C. For RT total strain, Nb, V, and Group IV elements Ti, Hf and Zr are key contributors, with Ta having a small positive influence. (Fig. 12c). The other alloying element in this study, especially Al, tends to reduce room temperature ductility. Interestingly, Cr appears to negatively influence both RT strain and HT strength, indicating that its higher concentrations may detract from the desired mechanical properties.

3.6. Navigating the compositional space

The MLR models developed here have been applied to show the relationships between RT ductility and HT strength at 1000 °C and 1200 °C. These properties have been estimated for over 35,000 hypothetical RCCAs drawn from the palette of the ten elements studied here (Al, Cr, Hf, Mo, Nb, Ta, Ti, V, W, and Zr). The mole fractions of the constituent elements are systematically varied from 0 to 0.4 in steps of 0.1 for ternary, quaternary and quinary RCCAs. The upper concentration limit was imposed to ensure all compositions remained within the range covered by the training dataset (Fig. 1). The results of these MLR predictions are shown in Fig. 13. Yellow markers represent the subset of 1-phase RCCAs from our refined dataset with experimentally measured HT strength but without measured RT ductility. For these alloys, RT ductility was inferred using our trained model. This analysis shows that most of the reported RCCAs fall well below the Pareto front and are not optimal compositions. A well-defined Pareto front shows the trade-off between HT strength and RT ductility for 1-phase RCCAs. Beyond illustrating the inevitable compromise between HT strength and RT ductility, this analysis also identifies over 50 promising RCCAs along the Pareto front (see Appendix). These candidate alloys, which theoretically offer an improved balance of HT strength and RT ductility over existing RCCAs, are pending experimental confirmation.

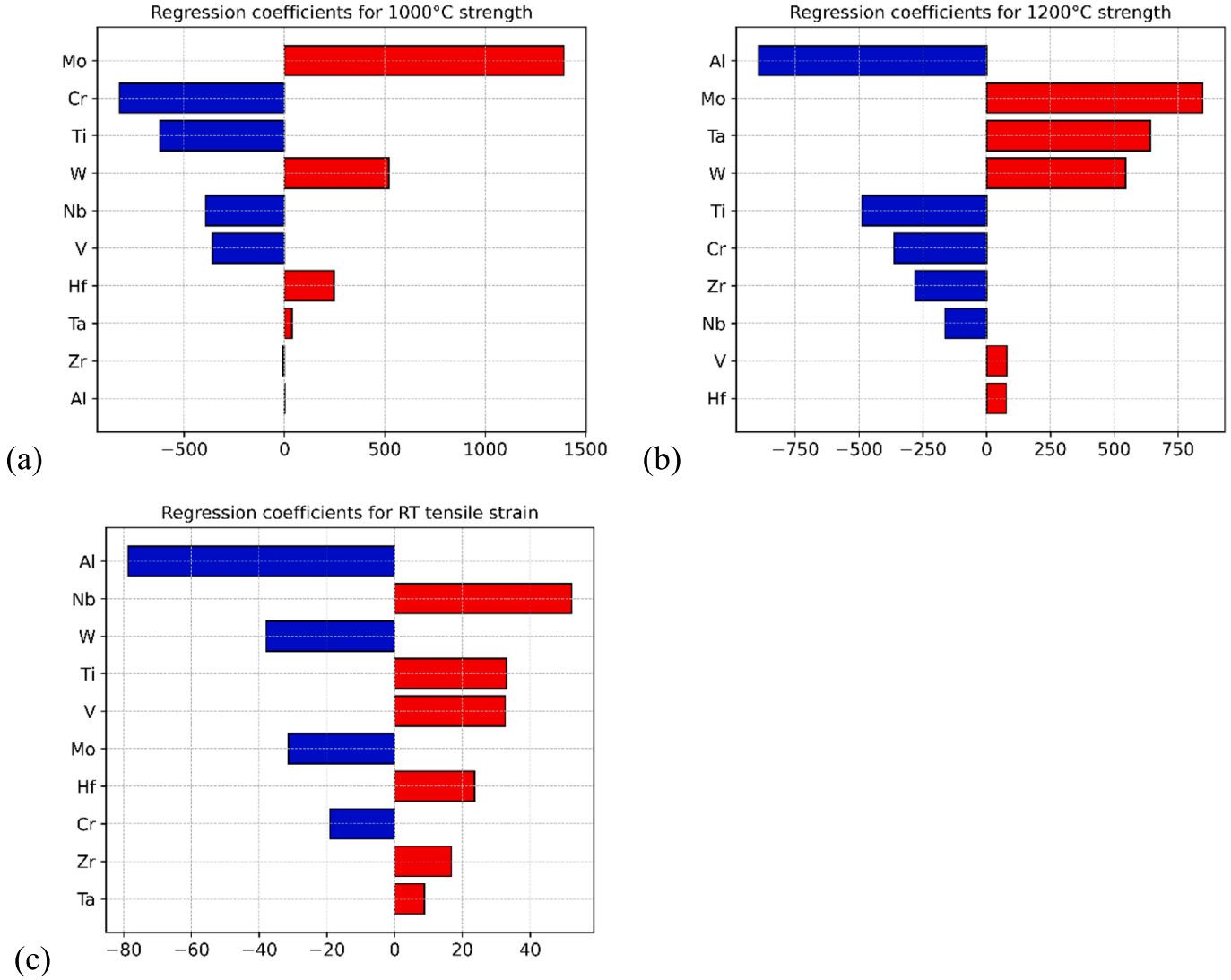

Fig. 12. Influence of alloying elements on (a) σ_y at 1000 °C, (b) σ_y at 1200 °C, and (c) RT total strain to failure in 1-phase RCCAs. The bars represent the regression coefficients of each element, indicating the magnitude and direction of their impact.

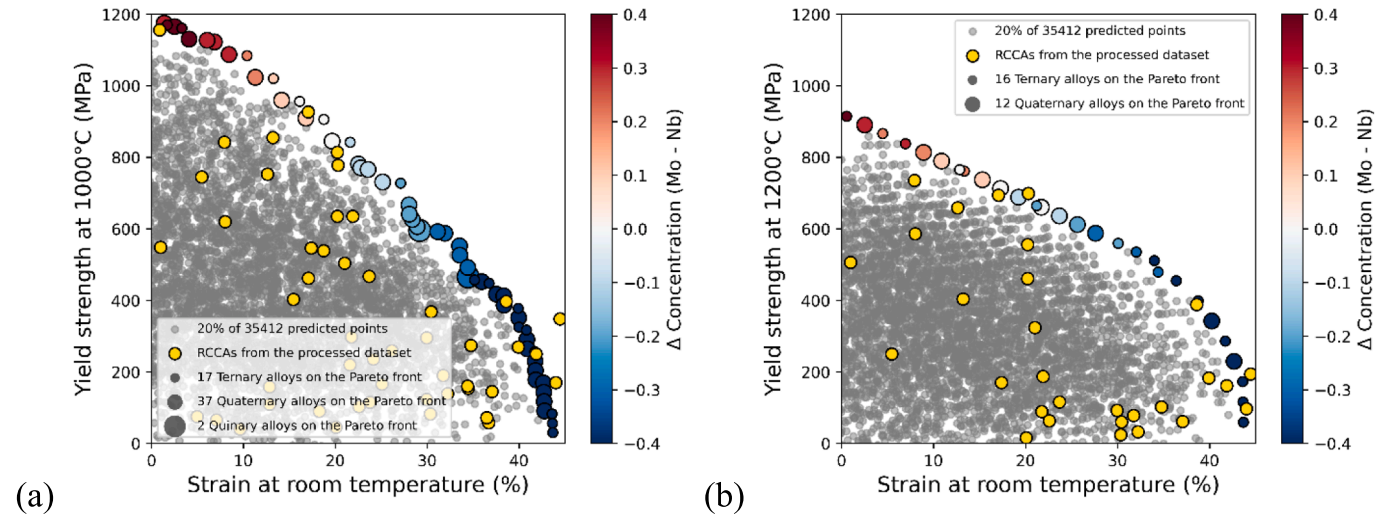

Fig. 13. Predicted RT strain and σ_y at (a) 1000 °C and (b) 1200 °C for ternary, quaternary and quinary RCCAs systematically drawn from the palette of ten elements in this study (Al, Cr, Hf, Mo, Nb, Ta, Ti, V, W, and Zr). The gray datapoints represent predicted σ_y and RT strain for 20 % of the 35,412 RCCAs predicted with the MLR model developed here. Yellow markers indicate RCCAs from our curated dataset, with measured σ_y and RT ductility predicted from the MLR model. The difference in atom fraction between Mo and Nb, $c_{Mo} - c_{Nb}$, is shown for some of the RCCAs on the Pareto front. (For interpretation of the references to color in this figure legend, the reader is referred to the web version of this article.)

These results emphasize the critical roles of Mo for HT strength and Nb for RT ductility by color-coding the composition difference, ($c_{Mo} - c_{Nb}$), along the Pareto front. This shows that RCCAs with more Mo than Nb tend to be stronger and have less ductility, while those with more Nb than Mo show the opposite trend. RCCAs with nearly equal amounts of Mo and Nb are found at the mid-span of the Pareto front, giving an attractive combination of both HT strength and RT ductility. The compositions of the RCCAs along the Pareto front predominantly feature Hf, Mo, Nb, Ta, and V, with the notable exclusion of Al, Cr and the infrequent use of W and Zr (Fig. 14).

4. Discussion

The correlations identified in the previous sections allow us to recommend an approach for selecting possibly ductile RCCAs with good HT strength. First, to achieve HT strength, a selected RCCA should have $T_L > 2100$ °C. The alloy should be a single-phase BCC structure or have secondary phases that are thermodynamically stable above the maximum use temperature. In the latter case, a single-phase solid solution range is desired below the $T_{solidus}$ for precipitation heat treatment. RCCAs that satisfy these thermodynamic properties can be found using CALPHAD methods. CALPHAD sometimes predicts secondary phases in

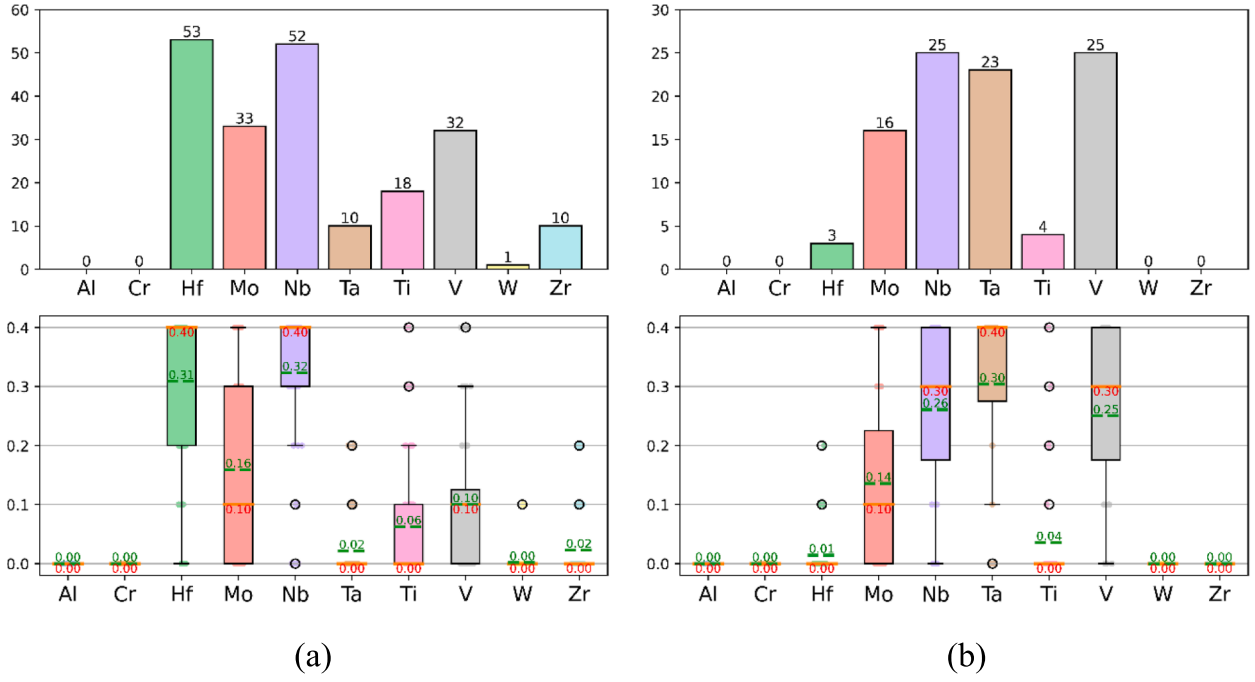

Fig. 14. The frequency (bar charts, upper panels) and concentration ranges (boxplots, lower panels) of the elemental constituents for RCCAs along the Pareto front in Fig. 13 at (a) 1000 °C and (b) 1200 °C. The boxplots show the concentration distribution for each element, with medians marked by red lines across the boxes and means by green dashed lines. Outliers are represented as individual points. (For interpretation of the references to color in this figure legend, the reader is referred to the web version of this article.)

RCCAs below 1000 °C that are not observed experimentally or require long-time annealing to form. Therefore, RCCAs with a 1- phase structure above 1000 °C can be considered to fall in the single-phase RCCA category. Additional criteria for RCCAs to have HT strength are VEC > 4.7 and density > 8 g/cm^3. These properties can be estimated using the rule of mixtures (ROM). To satisfy these criteria, it is likely that the prospective RCCAs should be rich with Nb, Ta, Mo and/or W. A positive effect of Mo on strength and stiffness of Mo-Nb-Ta-Ti RCCAs has recently been emphasized by Startt et al. [49] and explained this by partial replacement of soft metallic bonds with stronger covalent bonds.

Second, potentially ductile RCCAs can be identified as those with a RT yield stress below 1600 MPa. The RT yield stress can be estimated using currently available strengthening models developed for single-phase BCC RCCAs. These are the Maresca-Curtin edge dislocation strengthening model [33] and the Rao-Suzuki screw dislocation strengthening model [34]. These models accurately predict the yield stress of RCCAs in which edge or screw dislocations control σ_y. Among these two models, the strength-controlling mechanism is the one with a higher σ_y. The final selection can be made by running the strengthening models to identify RCCAs with predicted HT σ_y that meet or exceed the application requirement. The properties of the selected RCCAs can be verified through high throughput experiments. Particular attention should be made to minimize the concentration of interstitial elements (O and N) and to avoid segregation of these elements at grain boundaries.

The correlations provided here can guide the development of RCCAs that have both strength at HT and ductility at RT. However, some of the correlations show wide bands for ductility, so that a given indicator can produce RCCAs that are either brittle or ductile, for example as shown in the relationships between ductility and yield strength or VEC (Fig. 9). This may suggest a less direct relationship between ductility and the tracked property, where the suggested property is necessary but not sufficient for ductility. It is likely that an RCCA may be intrinsically capable of displaying plasticity, for example as suggested by the correlations in Fig. 10, but none is measured due to the presence of defects, microstructural inhomogeneities, or the intervention of a competing failure mode. Defects can include porosity or residual stresses; dendritic segregation of refractory elements is a major source of microstructural inhomogeneity; and competing failure modes may include bulk cleavage fracture or premature grain boundary decohesion due to interstitial segregation. Thermo-mechanical processing may reduce or eliminate many of these extrinsic effects, and the development of such processes is suggested to improve the balance of properties in RCCAs. TMP is expected to be particularly effective in removing residual stresses from casting; healing porosity; reducing or eliminating dendritic segregation of principal alloying elements; reducing segregation of interstitial elements at grain boundaries; and in producing a uniform distribution of refined grains. Supporting the suggestion for deformation processing, analysis of available datasets shows that RT tensile ductility in RCCAs generally improves after TMP [23].

We have recently successfully applied this approach for the development of a few ductile RCCAs which have yield stresses above 300 MPa at 1200 °C and promising ductility at room temperature. Some of these RCCAs are listed in Table 3. All the developed alloys that did not fracture after 50 % compression strain at RT, have RT yield stress below 1000 MPa. These alloys have a weak temperature dependence of yield stress in the temperature range from 25 °C to 1200 °C. R1-5, R2-2, R2-7 and GEX are M-phase RCCAs, which have relatively low compression ductility at RT but very attractive HT mechanical properties, which are in-line with their high T_L.

The MLR models developed here give an alternate approach to design RCCAs with a balance of RT ductility and HT strength. Elements that seem essential to simultaneously provide RT ductility and HT strength include Mo, Nb and V (Fig. 14a,b). Hf and Ti are also important at 1000 °C, while Ta is indicated at 1200 °C. Three alloys in the curated dataset used here fall on the mid-region of the Pareto front and five more are found on the high ductility end at 1000 °C; and four RCCAs cover the same extent of the Pareto front at 1200 °C. These previously published nearly optimal RCCAs at 1000 °C are HfMoNbTaZr, HfMoNbTaTiZr, HfMoNbTaTi, $Hf_{19}Nb_{74}W_6O_1$, $Nb_{64}Ti_{25}W_{11}$, $Mo_{0.21}NbTi_{0.27}$, $Mo_{0.17}NbTi_{0.26}$, $Mo_{0.13}NbTi_{0.24}$ and $NbTi_{0.25}W_{0.11}$, and at 1200 °C are HfMoNbTaTi, $Hf_{19}Nb_{74}W_6O_1$ and $NbTi_{0.25}W_{0.11}$ [35,38,50]. It is notable that all but one of these RCCAs have between 25 and 40 at. % Group IV elements, which may contribute to the balance of strength and ductility [32]. The one exception, $Hf_{19}Nb_{74}W_6O_1$, is a niobium alloy WC-3009, which contains an intentional oxygen addition that is five times higher than typical interstitial levels in refractory alloys [51].

Careful inspection of the RCCAs in Table 3 shows that many have a balance of RT compressive ductility and high temperature strength that meet or exceed the Pareto fronts in Fig. 13a,b. All but one of these RCCAs have compositions that are outside the bounds used to calculate the strength and ductility values in Fig. 13. Further, two of the already published RCCAs that fall along the Pareto fronts in Fig. 13 also have one element that is more concentrated than the 40 % limit used in the MLR model. This emphasizes the importance of extending RCCA efforts to include alloys with a dominant principal element.

The current correlations and MLR models are limited by the data currently available. Relatively few efforts have been published to design M-phase microstructures capable of producing both strength and ductility. Specifically, efforts to intentionally control the size, volume fraction, distribution and dissolution temperature of strengthening phases are infrequently undertaken. As a result, it may not be surprising that the current results suggest that 1-phase RCCAs currently offer the strongest potential to achieve this balance. A growing number of studies are exploring RCCAs with superalloy-like microstructures consisting of a disordered BCC (A2) phase and the related ordered B2 phase [52,53]. In addition to producing an attractive combination of size, volume fraction and distribution of second phases, these studies also strive to increase the dissolution temperature of the ordered B2 phase. Continued developments in this direction, as well as expanding to include other strengthening phases beyond B2, remain a relatively unexplored area of effort and is suggested for future work.

Table 3
Composition and properties (compression σ_y and ε_f at 25 °C and 1200 °C, ρ, T_L, VEC) of some RCCAs, which were developed using correlations reported in this study.

Alloy	ρ, g/cm^3	VEC	25 °C σ_y, MPa	25 °C ε_f, %	1200 °C σ_y, MPa	1200 °C ε_f, %	T_L, °C
$Nb_{74}Mo_{17}Zr_9$	8.58	5.08	632	>50	390	>50	2427
$Nb_{74}Mo_{12}Ti_5Zr_9$	8.33	4.98	690	>50	343	>50	2387
$Nb_{65}Ti_{18}Re_5W_{12}$	9.46	5.04	1000	14	337	>50	2450
MoReW	16.2	6.33	555	>50	325	>50	2879
R1-2 (Mo-Nb-Hf-Ti-Zr)	8.75	4.97	877	>50	394	>50	2388
R1-5 (Cr-Hf-Mo-Nb-Ti)	8.97	5.06	1250	12	480	>50	2292
R2-2 (Hf-Mo-Nb-Ti-Zr)	9.00	5.17	1200	10	608	>50	2428
R2-7 (Cr-Mo-Nb-Ti)	8.26	5.36	1365	10	648	35	2304
GEX (Hf-Mo-Re-Ru-W)	15.3	6.05	1322	12	810	30	2696

5. Summary and conclusions

Using experimental data in the open literature, the room temperature (RT) ductility and high-temperature (HT) strength of RCCAs are correlated against CALPHAD estimates of the liquidus temperature (T_L) and rule-of-mixtures (ROM) estimates for elastic properties, density (ρ) and valence electron concentration (VEC). RCCAs with high yield strengths above 1000 °C (e.g. ≥300 MPa at 1200 °C) generally have T_L > 2100–2200 °C; ρ > 8–10 g/cm^3; and VEC > 4.6–5.0. Among the currently reported RCCAs, only single-phase (1-phase) RCCAs containing Nb, Ta, Mo or W satisfy all three of these criteria. The reported multiphase (M-phase) RCCAs do not provide high strength above 1000 °C due to the relatively low T_L and the loss of strengthening near the solvus temperature of secondary phases. However, M-phase RCCAs are normally stronger than 1-phase RCCAs, even at high temperatures, when they both have the same T_L. Therefore, it is worth developing M-phase RCCAs with T_L > 2100–2200 °C that also have secondary phases that are stable at high temperatures.

RCCAs that are ductile at RT have yield strengths below 1600 MPa and VEC values from 4 to 5. RCCAs with extremely high RT yield strengths (>1600 MPa) are not attractive HT structural materials as they are brittle at RT and they lose strength rapidly above 1000 °C.

There is an approximate linear correlation between RT and elevated temperature yield strengths below ~0.55 T_L, likely due to the same operating strengthening mechanisms. This correlation is absent when the test temperature, T > 0.55 T_L, due to the operation of different strengthening mechanisms below and above 0.55 T_L and the related drop in strength near this homologous temperature.

A multivariate linear regression (MLR) model has been developed using machine learning in the high dimensional RCCA design space. This important contribution gives new insights, beyond traditional pairwise comparisons, into correlations between temperature-dependent material properties and the very high dimensional spaces of complex, concentrated compositions. The model effectively correlates experimentally-reported and MLR-predicted RT ductility and HT yield strengths, and identifies alloy compositions near the strength-ductility Pareto front that simultaneously optimize both of these properties. Only a few existing RCCAs are near this Pareto front – the current MLR model identifies many new prospective RCCAs for further exploration.

Data in the current literature continue to focus on cast materials. As a strong suggestion for future advancements, the development of thermo-mechanical processes is essential to improve ductility by reducing or eliminating defects and microstructural inhomogeneities that can lead to premature fracture.

CRediT authorship contribution statement

O.N. Senkov: Conceptualization, Methodology, Validation, Formal analysis, Investigation, Data curation, Visualization, Supervision, Writing – original draft, Writing – review & editing. **S. Gorsse:** Methodology, Software, Validation, Formal analysis, Data curation, Visualization, Writing – original draft, Writing – review & editing. **D.B. Miracle:** Conceptualization, Methodology, Validation, Writing – original draft, Writing – review & editing. **S.I. Rao:** Methodology, Formal analysis, Validation, Writing – review & editing. **T.M. Butler:** Project administration, Funding acquisition, Supervision, Writing – review & editing.

Declaration of competing interest

The authors declare that they have no known competing financial interests or personal relationships that could have appeared to influence the work reported in this paper.

Data availability

Data will be made available on request.

Acknowledgements

The authors acknowledge numerous discussions with Drs. E. Payton, S. Kuhr, C. Woodward, D. Lee, S.L. Semiatin, J.-P. Couzinie. O.N. Senkov and S.I. Rao acknowledge financial support through the United States Air Force on-site contract No. FA8650–21-D-5270 managed by MRL Materials Resources, LLC, Xenia, Ohio, USA. Alloys R1-2, R1-5, R2-2 and R2-7 were developed during ARPA E Ultimate program funded by Department of Energy, United States.

Appendix A. RCCA compositions and properties predicted on the 1000 °C Pareto front (Fig. 13a) using the MLR models

Alloy Composition (Moles)	σ_y at 1000 °C (MPa)	RT strain (%)
Hf0.4Mo0.1Nb0.3Ta0.1V0.1	596	29
Hf0.3Mo0.1Nb0.4Ti0.1V0.1	466	34
Hf0.4Mo0.4Nb0.1W0.1	1175	1
Hf0.4Mo0.1Nb0.4Zr0.1	588	32
Hf0.4Mo0.1Nb0.4V0.1	553	34
Hf0.4Mo0.1Nb0.4Ti0.1	526	34
Hf0.3Mo0.1Nb0.4V0.2	492	34
Hf0.4Nb0.4Ta0.1Zr0.1	452	36
Hf0.4Nb0.4Ta0.1V0.1	417	38
Hf0.4Nb0.4V0.1Zr0.1	413	38
Hf0.2Mo0.2Nb0.4V0.2	606	29
Hf0.4Nb0.4Ti0.1Zr0.1	386	38
Hf0.3Nb0.4Ti0.1V0.2	291	41
Hf0.3Nb0.4Ti0.2V0.1	264	41
Hf0.2Nb0.4Ti0.1V0.3	230	42
Hf0.2Nb0.4Ti0.2V0.2	204	42
Hf0.2Nb0.4Ti0.3V0.1	178	42
Hf0.1Nb0.4Ti0.1V0.4	169	43
Hf0.1Nb0.4Ti0.2V0.3	143	43
Hf0.1Nb0.4Ti0.3V0.2	117	43
Hf0.1Nb0.4Ti0.4V0.1	91	43
Hf0.4Nb0.4Ti0.1V0.1	351	40
Hf0.4Mo0.1Nb0.3Zr0.2	626	28
Hf0.4Mo0.1Nb0.4Ta0.1	592	31

(continued on next page)

(*continued*)

Alloy Composition (Moles)	σ_y at 1000 °C (MPa)	RT strain (%)
Hf0.3Mo0.2Nb0.4V0.1	667	28
Hf0.4Mo0.4Nb0.1V0.1	1088	8
Hf0.3Mo0.2Nb0.4Ti0.1	641	28
Hf0.2Mo0.4Nb0.3V0.1	960	14
Hf0.4Mo0.4Nb0.1Zr0.1	1123	7
Hf0.4Mo0.3Nb0.2V0.1	909	17
Hf0.4Mo0.4Nb0.1Ta0.1	1127	6
Hf0.4Mo0.4Ta0.1V0.1	1131	4
Hf0.3Mo0.4Nb0.2V0.1	1024	11
Hf0.4Mo0.4Ta0.1Zr0.1	1166	3
Hf0.2Mo0.3Nb0.4V0.1	781	23
Hf0.4Mo0.2Nb0.3Ta0.1	771	23
Hf0.4Mo0.2Nb0.3Zr0.1	766	24
Hf0.4Mo0.2Nb0.3V0.1	731	25
Hf0.3Mo0.3Nb0.3V0.1	845	20
Hf0.4Mo0.4Nb0.2	1084	10
Hf0.4Mo0.4Ta0.2	1170	2
Nb0.4Ti0.2V0.4	82	44
Hf0.2Nb0.4V0.4	256	42
Hf0.4Mo0.4Zr0.2	1161	3
Hf0.4Nb0.4V0.2	377	40
Hf0.4Nb0.4Ti0.2	325	40
Hf0.3Mo0.4Nb0.3	1020	13
Hf0.2Mo0.4Nb0.4	956	16
Hf0.4Nb0.4Zr0.2	448	37
Hf0.4Mo0.3Nb0.3	906	19
Hf0.4Nb0.4Ta0.2	457	35
Hf0.3Mo0.3Nb0.4	842	22
Nb0.4Ti0.3V0.3	56	44
Hf0.4Mo0.2Nb0.4	728	27
Hf0.3Nb0.4V0.3	317	41
Nb0.4Ti0.4V0.2	30	44

Appendix B. RCCA compositions and properties predicted on the 1200 °C Pareto front (Fig. 13b) using the MLR models

Alloy Composition (Moles)	σ_y at 1200 °C (MPa)	RT strain (%)
Mo0.1Nb0.2Ta0.4V0.3	636	24
Mo0.1Nb0.4Ta0.4V0.1	588	28
Mo0.1Nb0.3Ta0.4V0.2	612	26
Mo0.1Nb0.1Ta0.4V0.4	660	22
Mo0.2Nb0.3Ta0.4V0.1	689	19
Mo0.2Nb0.2Ta0.4V0.2	713	17
Hf0.1Nb0.4Ta0.1V0.4	342	40
Mo0.2Nb0.1Ta0.4V0.3	737	15
Mo0.3Nb0.2Ta0.4V0.1	790	11
Mo0.3Nb0.1Ta0.4V0.2	814	9
Hf0.1Nb0.4Ti0.1V0.4	229	43
Mo0.4Nb0.1Ta0.4V0.1	890	3
Nb0.3Ta0.3V0.4	479	34
Nb0.4Ta0.2V0.4	399	39
Nb0.4Ta0.3V0.3	455	36
Nb0.4Ti0.2V0.4	173	44
Hf0.2Nb0.4V0.4	286	42
Nb0.4Ta0.4V0.2	511	34
Mo0.4Ta0.4V0.2	915	1
Nb0.2Ta0.4V0.4	559	30
Nb0.4Ti0.3V0.3	116	44
Mo0.2Nb0.4Ta0.4	664	21
Mo0.2Ta0.4V0.4	761	13
Mo0.3Nb0.3Ta0.4	765	13
Mo0.3Ta0.4V0.3	838	7
Mo0.4Nb0.2Ta0.4	866	4
Nb0.3Ta0.4V0.3	535	32
Nb0.4Ti0.4V0.2	59	44

References

[1] P. Tsakiropoulos, Beyond Nickel Based Superalloys, Encyclopedia of Aerospace Engineering, John Wiley & Sons, Oxford, UK, 2010.

[2] J.H. Perepezko, The hotter the engine, the better, Science 326 (5956) (2009) 1068–1069.

[3] O.N. Senkov, D.B. Miracle, K.J. Chaput, J.-P. Couzinie, Development and exploration of refractory high entropy alloys - A review, J. Mater. Res. 33 (19) (2018) 3092–3128.

[4] J.-W. Yeh, S.-K. Chen, S.-J. Lin, J.-Y. Gan, T.-S. Chin, T.-T. Shun, C.-H. Tsau, S.-Y. Chang, Nanostructured high-entropy alloys with multiple principal elements: Novel alloy design concepts and outcomes, Adv. Eng. Mat. 6 (5) (2004) 299–303.

[5] B. Gorr, S. Schellert, F. Muller, H.-J. Christ, A. Kauffmann, M. Heilmaier, Current status of research on the oxidation behavior of refractory high entropy alloys, Adv. Eng. Mat. 23 (5) (2021).

[6] M. Abubaker Khan, T.-L. Wang, C. Feng, H. Sun, B. Wang, M. Hamza, G. Yasin, M. A. Afifi, W.-B. Liao, A superb mechanical behavior of newly developed lightweight and ductile Al0.5Ti2Nb1Zr1Wx refractory high entropy alloy via nano-precipitates and dislocations induced-deformation, Mater. Des. 222 (2022).

[7] Y. Gao, K. Chong, L. Qiao, Y. Li, C. Liu, F. Guo, D. Wu, Y. Zou, Synthesis and corrosion behavior of Mo15Nb20Ta10Ti35V20 refractory high entropy alloy, Mater. Des. 228 (2023) 111820.

[8] S. Gorsse, D.B. Miracle, O.N. Senkov, Mapping the world of complex concentrated alloys, Acta Mater. 135 (2017) 177–187.

[9] O.N. Senkov, S.V. Senkova, D.M. Dimiduk, C. Woodward, D.B. Miracle, Oxidation behavior of a refractory NbCrMo0.5Ta0.5TiZr alloy, J. Mater. Sci. 47 (18) (2012) 6522–6534.

[10] O.N. Senkov, G.B. Wilks, D.B. Miracle, C.P. Chuang, P.K. Liaw, Refractory high-entropy alloys, Intermetallics 18 (2010) 1758–1765.

[11] O.N. Senkov, S. Gorsse, D.B. Miracle, High temperature strength of refractory complex concentrated alloys, Acta Mater. 175 (2019) 394–405.

[12] O.N. Senkov, D.B. Miracle, S.I. Rao, Correlations to improve room temperature ductility of refractory complex concentrated alloys, Mater. Sci. Eng. A 820 (2021) 141512.

[13] C.-J. Liu, C. Gadelmeier, S.-L. Lu, J.-W. Yeh, H.-W. Yen, S. Gorsse, U. Glatzel, A.-C. Yeh, Tensile creep behavior of HfNbTaTiZr refractory high entropy alloy at elevated temperatures, Acta Mater. 237 (2022).

[14] L. Xu, Y. Jia, S. Wu, Y. Mu, Y. Jia, G. Wang, Low cycle fatigue properties of refractory high-entropy HfNbTiZr alloy, Intermetallics 152 (2023).

[15] P.K. Liaw, S. Chen, K.-K. Tseng, J.-W. Yeh, T. Liu, F. Meng, Remarkable high-cycle fatigue resistance of the TiZrNbHfTa high-entropy alloy and associated mechanisms, SSRN Electron. J. 1 (2020) u201343.

[16] X. Yin, Y.-K. Dou, X.-F. He, K. Jin, C.-L. Wang, Y.-G. Dong, C.-Y. Wang, Y.-F. Xue, W. Yang, Effects of Nb addition on charpy impact properties of TiVTa refractory high-entropy alloy, Acta Metallurgica Sinica (English Letters) 36 (3) (2023) 405–416.

[17] P. Kumar, S.J. Kim, Q. Yu, J. Ell, M. Zhang, Y. Yang, J.Y. Kim, H.-K. Park, A. M. Minor, E.S. Park, R.O. Ritchie, Compressive vs. tensile yield and fracture toughness behavior of a body-centered cubic refractory high-entropy superalloy Al0.5Nb1.25Ta1.25TiZr at temperatures from ambient to 1200C, Acta Mater. 245 (2023).

[18] S. Zeng, Y. Zhu, W. Li, H. Zhang, H. Zhang, Z. Zhu, A single-phase Ti3Zr1.5NbVAl0.25 refractory high entropy alloy with excellent combination of strength and toughness, Mater. Lett. 323 (2022).

[19] X.J. Fan, R.T. Qu, Z.F. Zhang, Remarkably high fracture toughness of HfNbTaTiZr refractory high-entropy alloy, J. Mater. Sci. Technol. 123 (2022) 70–77.

[20] S. Gorsse, M.H. Nguyen, O.N. Senkov, D.B. Miracle, Database on the mechanical properties of high entropy alloys and complex concentrated alloys, Data Brief 21 (2018) 2664–2678.

[21] J.P. Couzinié, O.N. Senkov, D.B. Miracle, G. Dirras, Comprehensive data compilation on the mechanical properties of refractory high-entropy alloys, Data Brief 21 (2018) 1622–1641.

[22] C.K.H. Borg, C. Frey, J. Moh, T.M. Pollock, S. Gorsse, D.B. Miracle, O.N. Senkov, B. Meredig, J.E. Saal, Expanded dataset of mechanical properties and observed phases of multi-principal element alloys, Sci. Data 7 (1) (2020).

[23] N. Yurchenko, E. Panina, A. Tojibaev, V. Novikov, G. Salishchev, S. Zherebtsov, N. Stepanov, Tuning the grain and domain sizes to achieve superior room-temperature tensile ductility in a B2-ordered refractory Al15Nb40Ti40V5 medium-entropy alloy, Mater. Sci. Eng. A 874 (2023) 145073.

[24] J.O. Andersson, T. Helander, L. Höglund, P.F. Shi, B. Sundman, Thermo-Calc and DICTRA, Computational tools for materials science, Calphad 26 (2002) 273–312.

[25] W. Cao, S.-L. Chen, F. Zhang, K. Wu, Y. Yang, Y.A. Chang, R. Schmid-Fetzer, W. A. Oates, PANDAT software with PanEngine, PanOptimizer and PanPrecipitation for multicomponent phase diagram calculation and materials property simulation, Calphad 33 (2) (2009) 328–342.

[26] S. Zheng, W. Feng, S. Wang, Elastic properties of high entropy alloys by MaxEnt approach, Comput. Mater. Sci 142 (2018) 332–337.

[27] L.-Y. Tian, G. Wang, J.S. Harris, D.L. Irving, J. Zhao, L. Vitos, Alloying effect on the elastic properties of refractory high-entropy alloys, Mater. Des. 114 (2017) 243–252.

[28] H.W. Yao, J.W. Qiao, J.A. Hawk, H.F. Zhou, M.W. Chen, M.C. Gao, Mechanical properties of refractory high-entropy alloys: experiments and modeling, J. Alloys Cmpds 696 (2017) 1139–1150.

[29] S. Huang, F. Tian, L. Vitos, Elasticity of high entropy alloys from ab initio theory, J. Mater. Res. 33 (19) (2018) 2938–2953.

[30] H.O. Mosca, G. Bozzolo, Surface energies of the solid solutions between Ti, V, Cr, Zr, Nb, Mo, Hf, Ta and W, Surf. Sci. 601 (2007) 3224–3232.

[31] C. Sammut, G.I. Webb, Encyclopedia of Machine Learning, Springer, Boston, MA, 2011.

[32] D.B. Miracle, O.N. Senkov, C. Frey, S. Rao, T.M. Pollock, Strength vs temperature for refractory complex concentrated alloys (RCCAs): A critical comparison with BCC elements and dilute alloys, Acta Mater. 266 (2024) 119692.

[33] F. Maresca, W.A. Curtin, Mechanistic origin of high strength in refractory BCC high entropy alloys up to 1900K, Acta Mater. 182 (2020) 235–249.

[34] S.I. Rao, C. Woodward, B. Akdim, O.N. Senkov, D. Miracle, Theory of solid solution strengthening of BCC chemically complex alloys, Acta Mater. 209 (2021) 116758.

[35] K.-K. Tseng, C.-C. Juan, S. Tso, H.-C. Chen, C.-W. Tsai, J.-W. Yeh, Effects of Mo, Nb, Ta, Ti, and Zr on mechanical properties of equiatomic Hf-Mo-Nb-Ta-Ti-Zr alloys, Entropy 21 (2019) 15.

[36] Z.D. Han, N. Chen, S.F. Zhao, L.W. Fan, G.N. Yang, Y. Shao, K.F. Yao, Effect of Ti additions on mechanical properties of NbMoTaW and VNbMoTaW refractory high entropy alloys, Intermetallics 84 (2017) 153–157.

[37] O.N. Senkov, G.B. Wilks, J.M. Scott, D.B. Miracle, Mechanical properties of $Nb_{25}Mo_{25}Ta_{25}W_{25}$ and $V_{20}Nb_{20}Mo_{20}Ta_{20}W_{20}$ refractory high entropy alloys, Intermetallics 19 (2011) 698–706.

[38] O.N. Senkov, S.I. Rao, T.M. Butler, K.J. Chaput, Ductile Nb alloys with reduced density and cost, J. Alloys Cmpds 808 (2019) 151685.

[39] O.N. Senkov, D.B. Miracle, Generalization of intrinsic ductile-to-brittle criteria by Pugh and Pettifor for materials with a cubic crystal structure, Sci. Rep. 11 (1) (2021).

[40] J.R. Rice, R. Thomson, Ductile versus brittle behaviour of crystals, Phil. Mag. 29 (1) (1974) 73–97.

[41] S. Sheikh, S. Shafeie, Q. Hu, J. Ahlstrom, C. Persson, J. Vesely, J. Zyka, U. Klement, S. Guo, Alloy design for intrinsically ductile refractory high-entropy alloys, J. Appl. Phys. 120 (16) (2016) 164902.

[42] C. Zhang, B.E. MacDonald, F. Guo, H. Wang, C. Zhu, X. Liu, Y. Kang, X. Xie, Y. Zhou, K.S. Vecchio, E.J. Lavernia, Cold-workable refractory complex concentrated alloys with tunable microstructure and good room-temperature tensile behavior, Scr. Mater. 188 (2020) 16–20.

[43] S.-P. Wang, E. Ma, J. Xu, New ternary equi-atomic refractory medium-entropy alloys with tensile ductility: Hafnium versus titanium into NbTa-based solution, Intermetallics 107 (2019) 15–23.

[44] Y. Yuan, Y. Wu, Z. Yang, X. Liang, Z. Lei, H. Huang, H. Wang, X. Liu, K. An, W. Wu, Z. Lu, Formation, structure and properties of biocompatible TiZrHfNbTa high-entropy alloys, Mater. Res. Lett. 7 (2019) 225–231.

[45] Z.Q. Xu, Z.L. Ma, Y. Tan, X.W. Cheng, Designing TiVNbTaSi refractory high-entropy alloys with ambient tensile ductility, Scripta Mater. 206 (2022) 114230.

[46] J. Zyka, J. Malek, J. Vesely, F. Lukac, J. Cízek, J. Kuriplach, O. Melikhova, Microstructure and room temperature mechanical properties of different 3 and 4 element medium entropy alloys from HfNbTaTiZr system, Entropy 21 (2019) 114.

[47] Z. Han, L. Meng, J. Yang, G. Liu, J. Yang, R. Wei, G. Zhang, Novel BCC VNbTa refractory multi-element alloys with superior tensile properties, Mater. Sci. Eng. A 825 (2021) 141908.

[48] N. Jia, Y. Li, X. Liu, Y. Zheng, B. Wang, J. Wang, Y. Xue, K. Jin, Thermal stability and mechanical properties of low-activation single-phase Ti-V-Ta medium entropy alloys, JOM (2019) 3490–3498.

[49] J. Startt, A. Kustas, J. Pegues, P. Yang, R. Dingreville, Compositional effects on the mechanical and thermal properties of MoNbTaTi refractory complex concentrated alloys, Mater. Des. 213 (2022) 110311.

[50] F.G. Coury, M. Kaufman, A.J. Clarke, Solid-solution strengthening in refractory high entropy alloys, Acta Mater. 175 (2019) 66–81.

[51] C.C. Wojcik, Thermomechanical Processing and Properties of Niobium Alloys, Niobium Science & Technology: Proceedings of the International Symposium Niobium 2001, TMS, Orlando, FL, 2001.

[52] D.B. Miracle, M.H. Tsai, O.N. Senkov, V. Soni, R. Banerjee, Refractory high entropy superalloys (RSAs), Scr. Mater. 187 (2020) 445–452.

[53] O.N. Senkov, J.K. Jensen, A.L. Pilchak, D.B. Miracle, H.L. Fraser, Compositional variation effects on the microstructure and properties of a refractory high-entropy superalloy AlMo0.5NbTa0.5TiZr, Mater. Des. 139 (2018) 498–511.